Resistive gas sensors based on metal-oxide nanowires

Ali Mirzaei, Jae-Hyoung Lee, Matthieu Weber, Mikhael Bechelany, Hyoun Woo Kim, Sang Sub Kim

JOURNAL OF APPLIED PHYSICS XX, XX (2019)

Tutorial: Resistive gas sensors based on metal oxide nanowires

Ali Mirzaei[1,a)], Jae-Hyoung Lee[2], Matthieu Weber[5], Mikhael Bechelany[5,b)], Hyoun Woo Kim[3,4,c)], Sang Sub Kim[2,d)]

[1]Department of Materials Science and Engineering, Shiraz University of Technology, Shiraz 715557-13876, Iran

[2]Department of Materials Science and Engineering, Inha University, Incheon 22212, Korea

[3]The Research Institute of Industrial Science, Hanyang University, Seoul 04763, Korea

[4]Division of Materials Science and Engineering, Hanyang University, Seoul 133-791, Korea

[5]Institut Européen des Membranes, IEM – UMR 5635, ENSCM, CNRS, University of Montpellier, Place Eugène Bataillon, 34095 Montpellier cedex 5, France

Authors to whom correspondence should be addressed: [a)]alimirzaei@sutech.ac.ir. [b)]mikhael.bechelany@umontpellier.fr [c)]hyounwoo@hanyang.ac.kr [d)]sangsub@inha.ac.kr

Abstract

Gas sensors are essential for industry and for a wide range of applications. They are for examples applied in public safety, pollution monitoring, and various industrial processes. Among the different gas sensing technologies, semiconducting metal oxide-based gas sensors are the most popular because of their low price, high sensitivity, short response time, high stability and simple operation. In these gas sensors, because gas adsorption has a direct relationship with the surface area of the sensing material, a higher surface area will result in a higher sensing response. Therefore, along with simple synthesis methods, nanowires (NWs) have recently gained special attention for the realization of gas sensors. In this tutorial review, the synthesis of metal oxide NWs, the fabrication of gas sensors and their sensing mechanisms are discussed. Different gas sensors such as single NW, noble metal functionalized NWs, heterojunctions NWs, self-heating NWs, UV-activated NWs and core-shell NWs are presented. This tutorial review aims to provide a broad vision for the researchers and students working in this upcoming field.

I. Toxic gases and vapors

Gases are intimately linked to life, as most of the living species continuously need to breathe air, which is basically a mixture of oxygen, nitrogen, argon, and other gases. In addition, many gases are used in our industrial era. For example, liquefied petroleum gas (LPG) is widely used in industry, as well as for cooking and heating purposes.[1] Even though LPG is not toxic, it is highly explosive.[2] Also, hydrogen gas is seen as the next "green fuel" and is currently used in fuel cells, although it is highly explosive.[3,4] In addition to explosive gases, the sources of toxic and pollutant gases have been significantly increased in the recent years, and there are many toxic gases in our atmosphere.[5] Toxic gases can cause harm in low levels over long periods of time (chronic exposure) or in higher concentrations over short periods of time (acute exposure). The threshold limit value (TLV) has been defined as the maximum concentration of a gas, which is allowed for repeated exposure without resulting in adverse health effects.[6] For example, the TLV values for CO, NO_2 and H_2S gases are 50, 3 and 10 ppm, respectively.[6]

Based on the WHO (World Health Organization), air pollution is mainly due to toxic gases and caused around seven million premature deaths in 2012.[7] There are many toxic gases in our surrounding atmosphere. For example, carbon monoxide (CO) poisoning results in over 5000 deaths in the USA.[8] In Denmark, from 1995 to 2015, several hundred people passed away due to CO poisoning.[9] Also, in Iran, as a typical developing country, 836 deaths occurred in 2016due to CO poisoning.[10] CO has not any color, odor and taste,[11] and it has 240 times greater affinity for hemoglobin in comparison with oxygen. It forms carboxyhemoglobin, which leads to a reduced oxygen delivery to tissues and can cause tissue hypoxia.[8,12] Also, CO easily binds to cytochrome oxidase and leads to lactic acidosis, apoptosis and hypoxia.[12] Another example is nitrogen dioxide (NO_2), which has a highly oxidizing nature.[13] Along with CO, this gas is a major air pollutant which can form through burning of fossil fuels, car exhaust, or emissions from industrial factories.[14,15] Long-term exposure to NO_2 can result in inflammation of lung tissue, silo-filler's disease and bronchiolitis fibrosis obliterans. In addition, NO_2 released by jets in the atmosphere can cause the destruction of ozone layer.[14] Hydrogen sulfide (H_2S) is another highly poisonous gas, which can be produced from the bacterial decomposition of organic materials. Moreover, H_2S is produced as a by-product of many industries, including waste management, petroleum refining, and natural gas production.[16] In low concentrations (50 ppm), it can cause problems to the eyes and the respiratory system. When the concentration is doubled, H_2S gas can

paralyze the olfactory nerves, and disable the sense of odor. Long-term exposure to 250 ppm H_2S causes asphyxia, and may lead to suffocation. Exposure to 1000 ppm of H_2S paralyzes the respiratory nerve center and physical collapse may occur suddenly.[17] In addition, increased concentrations of H_2S are associated with chronic bronchitis, emphysema, pneumonia or cardiovascular system related diseases such as hypertension.[18]

Volatile organic compounds (VOCs) represent another major air pollutant. These organic compounds have a Reid vapor pressure of over 10.3 Pa at normal temperature (293.15 K) and pressure (101.325 kPa).[19] Examples are carbonyls, alkanes, esters, alcohols, alkenes, ethers, amides, and aromatics.[20] Most of VOCs cause atmospheric pollution and also are toxic to humans (carcinogenic, mutagenic, or teratogenic).[21-23] Accumulation of some VOCs can lead to Building-Related Illnesses (BRI) and the so-called sick building syndrome (SBS) which is responsible for the symptoms of headache and nausea.[24]

II. Gas sensors: General overview

Even though human olfaction system has long been considered the least significant of the human senses,[25] it has of high importance for our life as it warns us about potential air hazards. Also, it is the only active sense during sleep.[26,2728] The human olfactory system can discriminate approximately 400,000 odors.[29] In addition, human olfactory system is more sensitive than rodents and dogs for some odors.[30] However, when the concentration of a gas is very low or gas is odorless, it cannot be sensed by human olfactory system. Therefore, technological sensitive devices are necessary to detect the presence of the toxic and dangerous gases in our environment.

Traditionally, the mass spectrometer,[31] the gas chromatography,[32] flame ionization detector[33] and Fourier transform infrared spectrometer[34] instruments have been utilized for the detection and the analysis of toxic gases. These analytical devices are usually bulky, expensive and often require trained operators. Therefore, they are used in labs and for specific purposes.[35] Furthermore, these bulky instruments cannot be used for on-site measurements, and extensively limiting their widespread applications.

In contrast to bulky analytical instruments, gas sensors are typically small and do not need sample preparation.[36] Gas sensors are a subcategory of chemical sensors and based on the

International Union of Pure and Applied Chemistry (IUPAC), a general definition for a chemical sensor[37] is "a device that transforms chemical information, ranging from concentrations of a specific sample component to total composition analysis, into an analytically useful signal". Different gas sensors have been developed for the sensing of various toxic gases, such as SAW gas sensors,[38] electrochemical gas sensors,[39,40] optical gas sensors,[41,42] gasochromic gas sensors,[43,44] quartz crystal microbalance gas sensors,[45] catalytic gas sensors,[46,47] thermal conductivity gas sensors,[48,49] cataluminescence sensors,[45,50] and resistive-based gas sensors.[51,52] In this review paper, the different aspects of resistive-based metal oxide nanowire (NW) gas sensors which work based on the resistance changes in the presence of the target gases will be presented.

III. Metal oxide-based gas sensors: Brief history

Because they were found to be more sensitive than the other species evaluated, canaries birds were one of the first "gas sensing tools" used for the detection of carbon monoxide gas[53,54]. Obviously, manufactured gas sensors with high sensitivity and high availability are preferred to animals. Back to 1953, Brattain and Bardeen found a direct evidence for the existence of an electron depletion region at the free surface of germanium as a semiconducting material.[55] Then, in 1954, Heiland found a correlation between the electrical resistance of ZnO and hydrogen gas, when it was put in a hydrogen gas atmosphere.[56] Next, in 1962, Seiyama used ZnO as a gas sensor for detection of toluene, benzene, carbon dioxide, propane, ethyl ether, and ethyl alcohol gases.[57] It was the first real device which utilized the resistance change in a metal oxide semiconductor resulting from gas adsorption. In Japan, the greatest catastrophe in bottled gas supply occurred around 1962, and became a social problem. This situation led Taguchi to develop and patent (1962)[58] the stannic oxide sensor, and he subsequently established the Figaro Engineering company (1968).[59]

Resistive-based gas sensors are currently one of the most studied groups of gas sensors[60,61] and contribute to more than 20 % of gas sensor market.[62] Many companies such as Figaro, FIS, and MICS are offering this type of sensors.[63] So far, different binary, ternary[64] and more complex metal oxides[65] have been used for the realization of the resistive-based gas sensors. However, in general they can be either n- or p-type semiconductor.[66] According to Kim *et al*[67], SnO_2, ZnO,

TiO_2, WO_3, In_2O_3 and Fe_2O_3 (with n-type conductivity) are the most common metal oxides for realization of gas sensors. This is mainly due to the high mobility of electrons in n-type metal oxides. The mobility of conduction electrons (n-type oxides) is reportedly 160 and 200 and 100 $cm^2/V.s$ for SnO_2, ZnO, and In_2O_3, respectively.[68] On the other hand, the mobility of positive holes in p-type metal oxides is usually significantly less, as exemplified by the value of 0.2 $cm^2/V.s$ for NiO.[69] Actually, it has been reported that the response of p-type metal oxides are equal to square root of that of n-type metal oxides with the same morphology.[70] This is a reason why p-type oxides are not utilized as much as n-type metal oxides. However, p-type metal oxides with good catalytic properties are also used for sensing applications.[71] For example, the p-Co_3O_4-decorated In_2O_3 nanorods revealed a good response to ethanol gas due to high catalytic activity of p-Co_3O_4.[72] Also, Cr_2O_3 functionalized WO_3 gas sensor revealed a high response to ethanol, which was partially related to the good catalytic activation of Cr_2O_3 to ethanol gas.

Today, metal oxide gas sensors are widely applied to the detection of toxic gases and vapors for environmental control,[73] automotive industry,[74] biomedical applications,[75] and food industry.[76] A relatively new application of gas sensors is disease diagnosis, for example, exhaled breath testing, which is a diagnostic method for early detection of disease. It is not only non-invasive, but also safe and low cost.[77] It is known that toluene is a biomarker of lung cancer, ammonia to kidney disorder, hydrogen sulfide to Halitos, and formaldehyde to cardiovascular disease.[78] Therefore, by detecting the low concentrations of these gases, the associated disease can be diagnosed.

IV. Metal oxide-based gas sensors: Design

There are many configurations available for the designs of semiconducting-based gas sensors, and they can be categorized in three major classes (i) sintered pellet gas sensor,[79] (ii) thick film gas sensor[80] and (iii) thin film gas sensor.[81] The use of pellet gas sensors is hindered because their surface area is limited, leading to relatively low gas response.[82] Accordingly, most of gas sensors are fabricated as thin or thick films, with tubular or planar configurations[83] (Fig. 1). Such sensors are prepared by depositing a sensitive layer over an insulating substrate. The substrate has electrodes on its surface for the readout of sensor resistance.[73,84] Different techniques for the deposition of the sensing layer at the surface of substrate are possible, such as sol-gel, physical

vapor deposition (PVD), chemical vapor deposition (CVD), screen printing, spray pyrolysis, as reviewed by Fine *et al.*.[85] In addition, metallic heaters such as Pt, Pd, Ag, Pd-Ag are often used to increase the sensor temperature to the desirable one.[73,84] However, recently, due to high costs of metallic electrodes, some metal oxide electrodes such as CuO-mixed $CaCu_3Ru_4O_{12}$ have been used as electrode in the gas sensors.[86] Fig. 1 depicts the schematic representations of tubular and planar gas sensor configurations

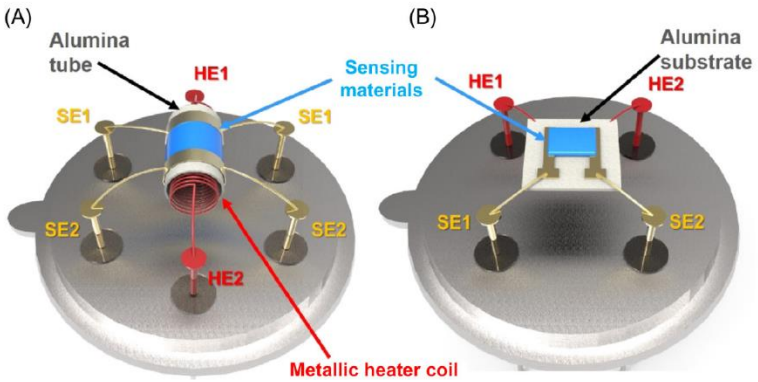

FIG.1.Schematic representations of gas sensor configuration (a) tubular and (b) planar gas sensors (SE and HE are sensor electrode and heater electrode, respectively).[83] Reproduced with permission from Technological realization of semiconducting metal oxide–based gas sensors. In *Gas Sensors Based on Conducting Metal Oxides*, 167-216 (2019). Copyright (2019) Elsevier.

Generally, alumina is used as the substrate material in gas sensors. This material has a low thermal expansion coefficient, high thermal conductivity, and high mechanical strength along with a low price.[83] Also, flexible gas sensors have become recently popular.[87,88] One of the most common substrates are plastics which are flexible, light weight, transparent, and can be mass produced by roll-to-roll printing processes.[83] Also, due to high working temperature of gas sensors, polyimide (PI), with a high thermal stability has been used as substrate material.[89]

V. Criteria of semiconducting gas sensor evaluation

In this section, the most important sensing parameters are introduced.

Gas response and sensitivity: The most important parameter of a gas sensor is its response to a target gas. It is obvious that if a gas sensor cannot sense a target gas, it cannot be practically used as a gas sensor. There are different definitions of gas response for semiconducting-based gas sensors. However, the ratio of resistance variation (R_a/R_g) or (R_g/R_a), where R_a and R_g are the resistance of gas sensor in air and in the target gas atmosphere respectively, is commonly used.[71] The former is used for an n-type metal oxide in the presence of a reducing gas such as CO or H_2S gas, or a p-type metal oxide in the presence of an oxidizing gas such as NO_2 gas. The latter is used for an n-type metal oxide in the presence of an oxidizing gas or a p-type metal oxide in the presence of a reducing gas. Therefore, in order to calculate and report the response of a gas sensor, its resistance in air (R_a) and target gas (R_g) should be continuously measured. This can be carried out using a gas sensing measuring system, which is discussed in the measuring systems section. For gas sensors, sensitivity (S) is the slope of response versus gas concentration curve.

Response time and recovery time: A gas sensor should produce a gas signal in the presence of a target gas as fast as possible. Response time is one of the main factors of the gas sensor, since if a gas sensor shows a good response to a target gas but with a long response time, it cannot be used in real applications. This is due to highly toxic or explosive nature of some target gases. By definition, response time is the required time for a gas sensor to reach to 90 % its final resistance in the presence of target gas.[90] In some literature a limit of 63 % of the stable resistance is reported for the response time.[91] Also recovery time is calculated as the time required for a gas sensor to reach its 10 % resistance value upon stoppage of target gas. A good strategy to improve the dynamic of gas sensors is use of porous structures for sensing layer, in which diffusion of gases species is accelerated.[92]

Selectivity (cross-sensitivity): Selectivity is another critical factor for a gas sensor. High selectivity means higher response of gas sensor to a target gas in comparison to the response to interfering gases.[93] Obtaining a high selectivity in a gas sensor is difficult since many gases have high cross-sensitivity which limits the practical usages of gas sensor.[94] The four common strategies for obtaining an increased selectivity are: (i) the functionalization with noble metal catalysts, (ii) tuning the sensing temperature (iii) using heterojunctions and additives and (iv)

filters.[95] In the recent years, the use of MOF as membranes has gained attention, as this new class of materials enable to enhance the selectivity as well.[96] These materials present functional pores that can lead to the specific separation of small molecules through several types of interactions including van der Waals interactions, metal-substrate interactions, and hydrogen bonding. Therefore, these materials have potential not only for gas separation and storage, but also for gas sensing.[97] Due to their adjustable pore sizes, these MOF can permit the selective separation of gas molecules.[97,98] Therefore, the precise engineering design of MOF coatings on the surface of sensing materials can lead to highly selective gas sensors.[99] For example, Weber *et al.* and Drobek *et al.*[100,101] covered ZnO NWs with a thin ZIF-8 molecular sieve membrane and reported high selectivity to H_2 gas. ZIF-8 membrane with a small pore size (3.4 Å) prevented passing of toluene and benzene gas molecules (kinetic diameters 5.92 and 5.27 Å, respectively), while H_2 molecules with smaller kinetic diameter (2.89 Å), diffused through the ZIF-8 membrane and resulted in a high response of gas sensor. Also, using sensor arrays, a high selectivity can be obtained by employing multiple sensing signal datasets [102]

Sensing temperature: The operating temperature of a gas sensor determines its sensitivity. Since the gas sensing phenomena are directly related to the diffusion and reaction of target gases and are temperature-dependent, the response of gas sensing increases with higher sensing temperatures. Generally, the working temperature of metal oxide gas sensors is in the range of 25 to 500 °C.[103] At low temperatures, the response is limited by the rate of chemical reactions while at high temperatures, it is limited by the diffusion rate of gas molecules. At intermediate temperatures, the rates of adsorption and desorption becomes equal and the highest response will be resulted. Every gas sensor shows its own optimal sensing temperature, which depends on the target gas, chemical composition, and morphology.[104] From an energy point of view, lower sensing temperatures are favorable since they request lower power consumption and allow the application of the gas sensor in remote areas. However, for some applications such as ammonia production industry which generally operates above 450 °C, high-temperature gas sensors are required.[105]

Limit of detection: The limit of detection can be calculated as "3 $noise_{rms}$/slope", in which $noise_{rms}$ is the standard deviation of the sensor signal, and the slope is the first derivative of the response versus the gas concentration.[106,107] Obviously, a lower limit of detection is desired.

VI. Measuring Systems

There are two general systems for gas sensing measurement: the dynamic and the static systems. Regardless the type of measuring system, the device requires the gas valves and gas flow controllers for the injection of the target gas into the gas chamber, equipped with a gas inlet and an outlet. The sensing temperature should be controllable, and a gas chamber with a limited volume in order to avoid long response times is typically preferred. Finally, the measuring system should be connected to a computer to continuously register the resistance of the sensor in different atmospheres.[17]

In a dynamic system (Fig. 2), pre-determined gas concentrations with constant flow rates, flow to the gas chamber through tubes by means of mass flow controllers.[108] The sensors that are inside the gas chamber are connected to the measurement unit to record the resistance variation continuously. During gas sensing tests, the resistance of the sensor in air and in the presence of different concentrations of target gas at different temperatures is recorded.

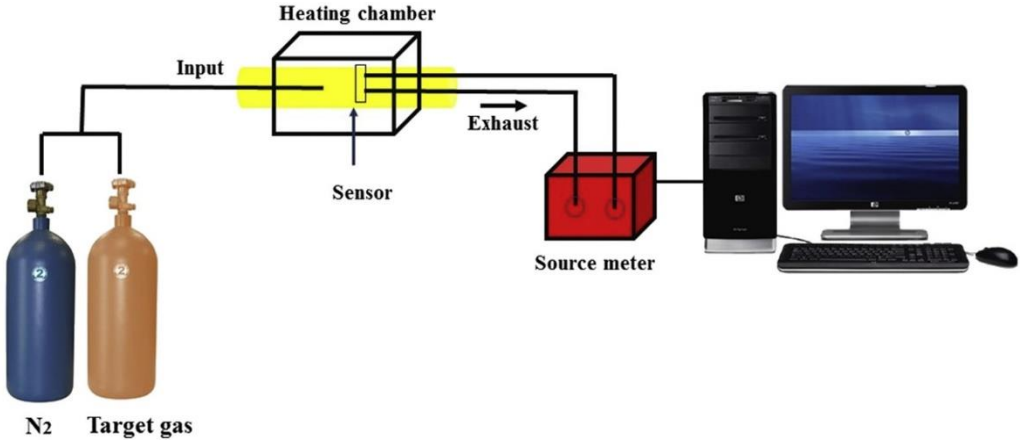

FIG. 2. Schematic representation of a dynamic gas sensing system.[108] Reproduced with permission from Thin Solid Films **636,** 257-266 (2017). Copyright (2019) Elsevier.

In the static sensing measurement system (Fig. 3), the sensor is put into a gas chamber with adjustable temperature and humidity.[109] During the gas sensing test, a pre-determined amount of the target gas is injected into the test chamber through the gas inlet by a gas injection unit. When the sensor resistance becomes stable, the gas chamber is opened to recover the sensors in air. For different gas concentrations and at different temperatures this procedure is repeated and a curve showing variations of sensors resistance versus time in different atmospheres will be obtained.

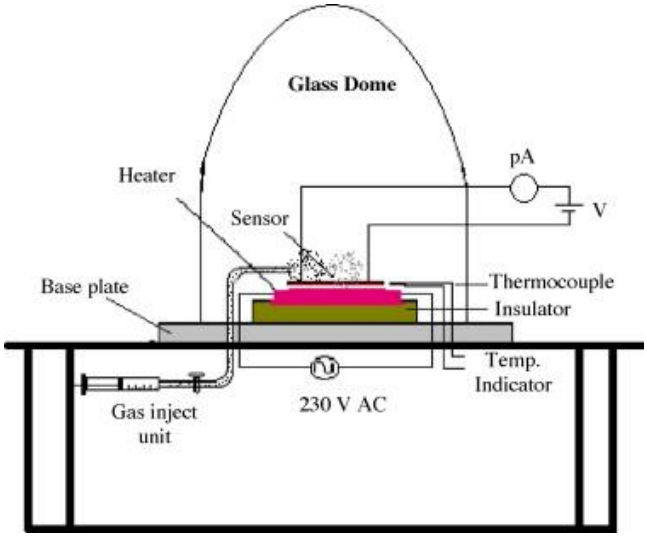

FIG. 3. Schematic representation of a static gas sensing system.[109] Reproduced with permission from Sensor. Actuat. B-Chem. **126**, 368-374 (2007). Copyright (2019) Elsevier.

VII. Nanowire-based gas sensors: General overview

The decrease of a sensor size will result in lower power consumption due to small thermal mass, mass production, quick heating and easier integration with small size chips.[83] Nanoscale materials not only present the above mentioned advantages but they also have a large effective area which is increasing the gas adsorption phenomena. When the size reaches λ_D (Debye length), the surface energy significantly increases and agglomeration easily occurs which results in the decrease of surface area.[71] One good approach to overcome the agglomeration is to engineer the surface at the nanoscale in order to increase the surface area of the gas sensor.[110] Therefore, various nanostructures such as nanowires (NWs),[111,112] nanofibers,[113,114] nanorods,[115,116] nanotubes,[117,118] hierarchical structures,[119,120] hollow structures,[121-123]

nanobelts,[124,125] mesoporous structures[126,127] and core-shell structures[128,129] have been explored for the preparation of gas sensing devices.

By definition, nanostructures which have cross-sections of between 2 to 200 nm with micrometer scale lengths are known as NW.[130] Using metal oxide NWs for the realization of gas sensors has advantages such as very large surface-to-volume ratio, low dimensions, high stability, high crystallinity, facile preparation methods, minimum power consumption, and ease of functionalization with catalysts for sensing studies.[68,131,132] Accordingly, NW gas sensors have been used not only for the realization of gas sensors,[133,134] but also for the fabrication of different kinds of biosensors.[135] In the next section we will discuss the synthesis of NWs and their performance as gas sensors briefly.

VIII. Synthesis of metal oxide NWs

The most common way to synthesize metal oxide NWs with random alignment is bottom-up approach, which can be classified into solution-phase growth and vapor-phase (solid-state) growth techniques. They are including solution-based techniques or template growth and synthesis by vapor phase transport or chemical vapor deposition. The advantages of these methods is high purity and small diameters of the materials synthesized, low cost synthesis and the ease of doping and homo- or heterojunctions formation.[131] The main disadvantage of the solution-based growth is the agglomeration of the NWs. The most common method for synthesis of NWs is vapor-liquid-solid (VLS) growth and we briefly explain VLS growth here.

Vapor-liquid-solid (VLS) growth: The bottom-up VLS growth was introduced by Wagner and Ellis at Bell Laboratories to describe the growth of Si whisker in the presence of a liquid gold droplet.[136] Compared to other growth techniques, the VLS is a simple and cheap method which is able to produce NWs with high aspect ratio.[137] Generally a metallic catalyst is used for VLS growth. Catalyst acts as a reservoir for atomic species and directs crystallization of NWs.[138] Generally, the length of NWs depends on the growth time, and the NW diameter are determined by the size of the metal catalyst droplets. If the size of catalysts has a narrow distribution, NWs with a uniform diameter can be obtained.

During a typical VLS growth technique, catalysts are first molten into liquid alloy droplets. Then, when the alloy droplets become supersaturated, source metal precipitates and metal oxides will be grown under the oxygen flow. As-synthesized metal oxides are grown along particular orientation, which lead to the formation of 1D NWs.[139] Considering the growth of TeO_2 NWs by a TeO_2 NWs and Au-catalyzed VLS growth technique as shown in Fig. 4, Au NPs were deposited on substrate on which TeO_2 NWs was grown. With the increasing amount of Te vapor condensation and dissolution, Te and Au form a liquid. With the decrease of temperature and in the presence of oxygen, the TeO_2 crystals nucleate and further condensation/dissolution of Te vapor increased the amount of TeO_2 crystal precipitation from the alloy. The incoming Te species diffused and condensed at the existing solid/liquid interface. As a result, no new solid/liquid interface was formed and the interface was pushed to form a TeO_2 NW. After cooling, the alloy droplets solidified on the TeO_2 NWs tips.[140,141] The reverse variation of VLS is the solid-liquid-vapor (SLV) growth method in which by etching a "negative NW", which is hollow in nature can be formed into a single crystal.[142]

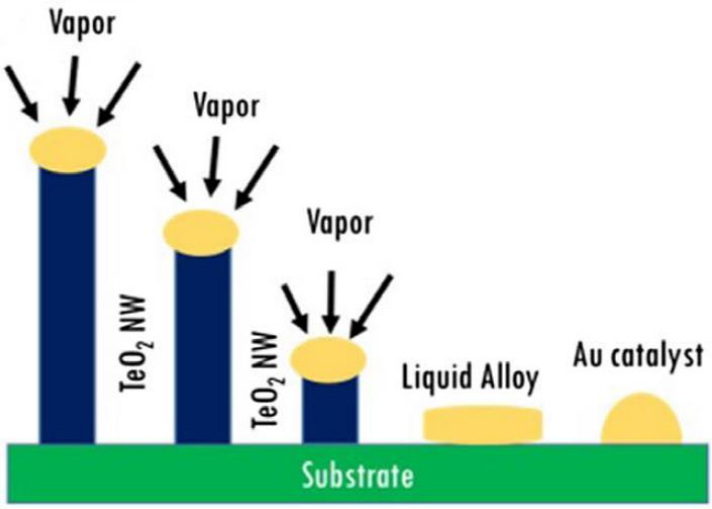

FIG. 4. Schematic representation of the VLS growth mechanism for TeO_2 NWs.[140] Reproduced with permission from Met. Mater. Inter. **25**, 805-813 (2018). Copyright (2019) Springer.

Synthesis of branched NW: Branched NWs, which also called nanoforests or nanotrees, have a three-dimensional (3D) morphology with a lot of homo- or hetero junctions and direct electron

transport pathways. Compared to NPs and 1D NWs, 3D branched NWs are superior in terms of structural hierarchy and high surface areas,[143] which facilitates their use for gas sensing studies even for detection of gases at sub-ppm level.[144] Also, branched NWs offer increased conduction paths and enhanced conduction between the NW branches and backbones.[145] Many methods can be used for the synthesis of branched NWs. Typical methods include sequential VLS solution growth on primary NWs, self-catalytic growth, and screw-dislocation in combination with VLS.[143] The most common method is VLS which consists of three steps namely VLS growth of the primary NWs, deposition of metal catalyst onto the primary NWs, and second VLS growth of the branched NWs. Density of the NW branches is directly related to the amount of the catalyst particles deposited on the primary NWs, while the length of the branches depends on the growth time.[143] Therefore, by VLS growth not only branched NWs with desired features can be synthesized, but also they have high crystal quality. However, synthesis temperature for VLS and most of vapor phase growth methods is high and some of them needs expensive facilities.[143]

Synthesis of core-shell NWs: The core-shell (C-S) NWs are a subcategory of composite materials which contain a NW core coated with one shell of different material. Therefore, C-S NWs are synthesized through the coating of an original core with a shell of other material. In C-S NWs, properties of resultant product can be different from either core or shell material.[147] The ideal synthesis method should be not only compatible with the procedure of realization of the gas sensor, but also be able to easily deposit the shell with high crystallinity and controlled thickness onto the core material. In addition, it should have minimal detrimental effects on the gas sensing performance of C-S NWs, be cost-effective, clean, and also safe.[147]

The bottom-up methods for synthesis of C-S NWs can enable for much finer structures and minimize energy loss compared with top down methods.[148] If various methods such as CVD or laser-induced assembly can be applied for the deposition of a shell material on a primary core NW, the most precise and reliable method is atomic layer deposition (ALD), which allows excellent control over the shell thickness.[149] ALD is a vapor phase technology based on the sequential use of self-limiting chemical reactions. This technique is able to produce inorganic nanomaterials such as oxides,[150] nitrides[151,152] and metals[153], with a subnanometer level control of the thickness.[154,155] The main benefits of the ALD route are the excellent control over the

thickness, the excellent uniformity and the conformality over the substrate surface, which makes this technique extremely appropriate for the coating of 1D materials such as NWs.[156-158] The shell layers produced by ALD are extremely smooth, continuous, pinhole-free and conformal to the original core, because the reactions are self-limiting and saturated.[155]

IX. Single NW gas sensors

Even though the development of single NW-based gas sensors is challenging, there are many reports about sensing properties of single NW-based gas sensors.[159-161] The sensing properties of single NWs are affected by the diameter, synthesis procedure and the reactions which that take place on their surfaces.[162] Realization of single NW gas sensors has considerable fabrication issues such as making electrical contacts. Electron-beam lithography can be used to define the electrical contacts for single NW gas sensor. However, a simpler method is synthesis, sonification and dispersal of NW on another substrate equipped with electrodes. Because of complex nature of processes, the commercialization of single NW gas sensors is very difficult.[163]

Tonezzer *et al.*[162] prepared monocrystalline SnO_2 NWs by CVD. They were subsequently dispersed onto a substrate and by applying of electrical contacts, the single NW gas sensors with different diameters were fabricated for NO_2 sensing studies (Fig. 5).

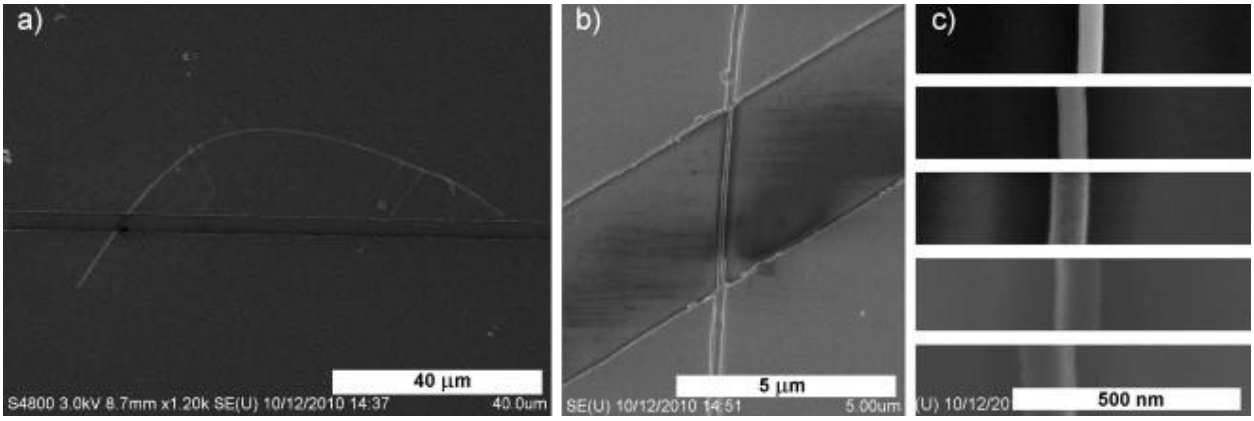

FIG. 5. (a), (b) SEM images of a single NW (c) and of NWs with different diameters (from the bottom to the top: 117, 103, 78, 62, and 41 nm).[162] Reproduced with permission from Sensor. Actuat. B-Chem. **163**, 146-152 (2012). Copyright (2019) Elsevier.

Fig. 6(a) shows the response of single NW gas sensors at the optimal temperature (200 °C). The gas sensor with smaller NW diameter resulted in a higher response. The response to NO_2 gas has the following relation with diameter (R) of NW and the depth of the depleted zone (L_D):[162]

$$\text{Response} = \text{Constant} \times \left(\frac{R}{R-L_D}\right)^2 \quad (1)$$

As illustrated in Fig. 6(b), the gas sensor with smaller NW diameter showed higher response to NO_2 gas. Since the L_D was constant for all NW gas sensors, the reduction of NW diameter resulted in higher gas response because of the higher ratio of the cross-sections of the conducting NW. Also since the gas sensors had different charge carrier densities, they showed different limit of detection values as provided in inset of Fig. 6(a).

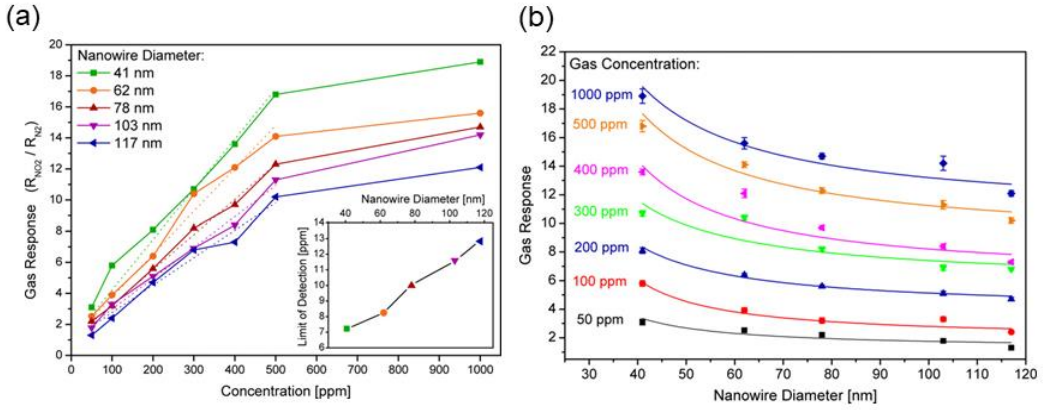

FIG. 6. (a) Gas responses of the five single NW sensors to various concentrations of NO_2 gas. Inset shows limit of detection for different single NW gas sensors (b) Gas responses versus NW diameter.[162] Reproduced with permission from Sensor. Actuat. B-Chem. **163**, 146-152 (2012), Copyright (2019) Elsevier.

The above results were also confirmed by Lupan group.[164] The response of single ZnO NWs (100 and 200 nm in diameter) gas sensors was directly related to the diameter of gas sensor and the highest gas response was occurred in a sensor of 100 nm in diameter. In the gas sensor with smaller diameter, the diameter and Debye length were almost comparable, which resulted in significant resistance modulation and a higher response of gas sensor.[164] In another study, the response of single SnO_2 NW gas sensors with different diameters (20-140 nm) were proportional

to inverse of diameter, where the NWs with smallest diameter, showed the highest gas response.[165]

In general, single NW gas sensors have weaker sensing properties than multiple or networked NW gas sensors. This is likely because of the presence of the large number of homojunctions in networked multiple NWs, acting as a powerful source of resistance modulation. In this regard, Zhang *et al.*[166] synthesized single In_2O_3 NW gas sensor by a laser ablation method. Single In_2O_3 NW demonstrated response to NO_2 down to ppb levels at ~25 °C. However, the response of multiple NW based gas sensor was not only higher, but also more reliable. Furthermore, the procedure for fabrication of multiple NW gas sensor was simpler.[166]

The addition of noble metals at the surfaces of single NW gas sensors also have been studied. Single ZnO NWs which were partially coated with Pt clusters showed good sensitivity and selectivity to hydrogen gas at room temperature, which was much better than uncoated sensor.[165] Also, the power consumption of single NW gas sensor was much lower than that of multiple ZnO NWs.[167]

X. Branched NW gas sensor

A high performance NO_2 gas sensor based on Bi_2O_3 branched SnO_2 NWs was reported by Bang *et al*.[168] The SnO_2 NWs as well as Bi_2O_3 branches were simultaneously produced by the VLS method. The sensor showed a high response of 56.92 to 2 ppm of NO_2 gas. The high sensing performance of the branched NW sensor was related to the high surface area of the sensor resulting from Bi_2O_3 branching and the formation of Bi_2O_3-Bi_2O_3 and SnO_2-SnO_2 homo-and Bi_2O_3-SnO_2 heterojunctions.

The CuO-functionalized SnO_2 branched NWs were realized in a single process using Cu as a catalyst for the growth of SnO_2 branches and the source of CuO NWs. By this method, Kim *et al.*,[169] fabricated NWs CuO-functionalized SnO_2 branched NWs. By annealing at 700 ^oC, the CuO was located at the tip of the SnO_2 branches. By exposing the gas sensor to H_2S, a high response was noticed which was mainly related to conversion of semiconductive CuO to metallic type CuS which induced significant resistance modulation. Also due to the fact that the CuO-induced depletion region covered a considerable volume of the SnO_2 branches, there was no

electron available for incoming NO_2 gas molecules, and a low response to NO_2 gas was resulted.[169]

Kim *et al.*[170], prepared ZnO branched SnO_2 NWs by a VLS growth method and then sputtered NWs with a Co shell followed by an annealing treatment to convert the cobalt layer to (Co) NPs at the ZnO branches surfaces (Fig. 7(a) and (b)). Figs. 7(c) and (d) show the schematics of the sensing mechanism in branched NWs gas sensors with and without Co-functionalization, respectively. The NO_2 gas molecules with highly oxidizing nature abstracted electrons from ZnO branches and led to higher resistance of gas sensors. However, for Co functionalized sensors, due to the spillover effect of Co, NO_2 gas species were first absorbed on the active sites of Co NPs and then migrated to the ZnO surfaces, contributing to an increase in resistivity. Furthermore, because of a difference between the work functions of n-ZnO and metallic Co, a Schottcky potential barrier formed on the interfaces between ZnO and Co. In NO_2 atmosphere, the gas molecules further take electrons from the Co, leading to the enlargement of the electron depletion layer in ZnO, and contributed to the sensor signal.

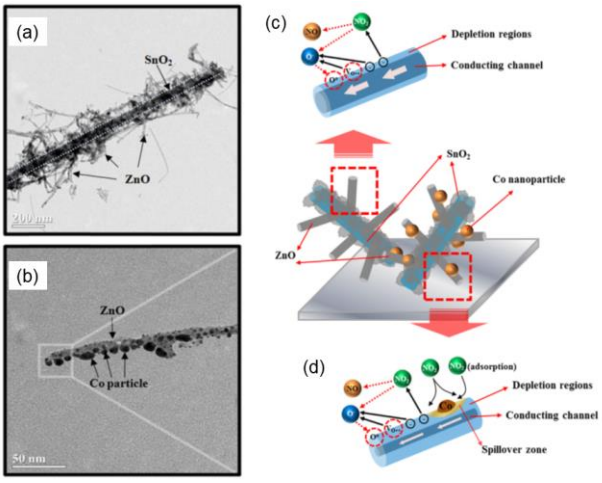

FIG. 7. TEM images showing (a) ZnO branches and (b) Co particles. Schematic of the sensing mechanisms (c) without and (d) with the Co-functionalization. Reproduced with permission from Sensor. Actuat. B-Chem. **219**, 22-29 (2015). Copyright (2019) Elsevier.

Woo *et al.*[171] prepared highly porous ZnO NWs by an Au-assisted VLS growth. Through the cation exchange reaction by thermal evaporation of $CoCl_2$ powder, as-grown ZnO NWs were

transformed into CoO NWs. The corresponding reaction resulted in the growth of co-deposited ZnO branches (Fig. 8).

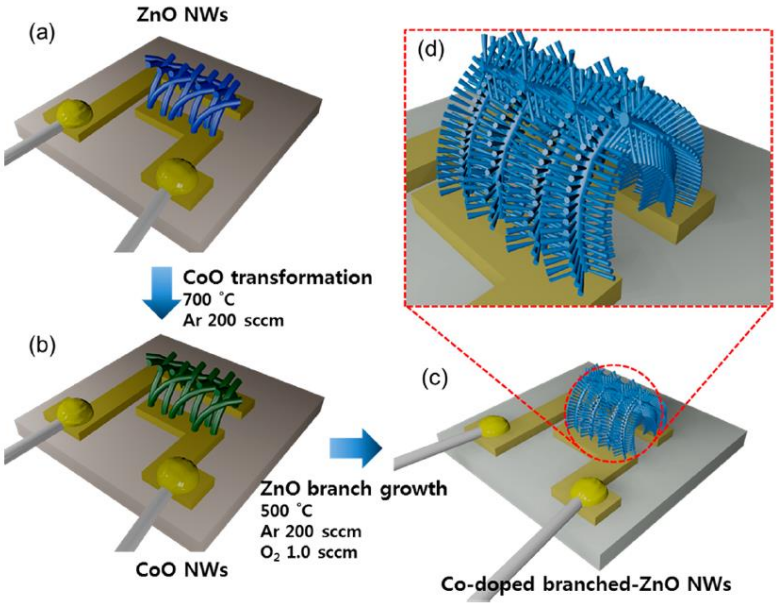

FIG. 8. (a) ZnO NWs (b) transformation of ZnO NWs into CoO NWs, (c, d) Co-doped ZnO NWs branched.[171] Reproduced with permission from ACS Appl. Mater. Interfaces **6**, 22553-22560 (2014). Copyright (2019) American Chemical Society.

In branched NWs, the presence of numerous homojunctions in ZnO branches resulted in higher initial resistance, compared to pristine ZnO NWs. Therefore, in the p-xylene atmosphere, a high modulation of resistance due to release of electrons, led to high response of gas sensor. In addition, the high response to p-xylene was also related to the catalytic activity of Co that facilitated the dissociation of the less reactive p-xylene to reactive smaller gases. In a similar study, Ni-doped branched ZnO NWs doped with Ni were grown by similar procedure described above. They showed enhanced gas response to 5 ppm p-xylene (R_a/R_g = 42.44) at 400 °C, which was significantly higher than the response to other gases. The high selectivity of gas sensor was related to the catalytic activity of Ni.[172]

An *et al.*[145], synthesized branched ZnO NWs using an Au-assisted VLS growth. The enhanced response to NO_2 gas over unbranched sensor was due to the three-dimensional porous structure and the high surface area owing to the formation of branches, along with presence of plenty of ZnO-ZnO homojunctions in branched morphology.

XI. C-S NW gas sensors

C-S composites have found special attention in many areas including catalysis and electrocatalysis[173] as well as different kinds of sensors.[174] Karnati *et al.* comprehensively discussed the different aspects of the sensing mechanism in C-S NWs gas sensors.[147] For gas sensing applications, generally an optimal shell thickness is needed to have the highest gas response in C-S NWs. This was confirmed by Kim *et al.*.[175] They reported the sensing performance of p-n CuO-ZnO C-S NWs with shell thicknesses of 5-110 nm. Gas sensing results showed the enhanced response to both C_6H_6 and CO gases at a shell thickness of 35 nm, which was closed to the Debye length (λ_D) of ZnO. For ZnO shells thinner than the λ_D of ZnO, all electrons were completely depleted (Fig. 9(a)) and in the presence of CO or C_6H_6 gases, the released electrons, significantly modulated the sensor resistance. For the shells thinner than the λ_D since the volume of the shell was much smaller than total volume of C-S NWs, negligible resistance modulations could not significantly affect the sensing response. Also, for the thick shells, only a portion of the shell experienced the resistance variations in air and target gas atmospheres, which resulted in low response of gas sensor. (Fig. 9(b)).

Also, in a similar study, the effect of shell thickness optimization on the sensing performance of SnO_2-Cu_2O C-S NWs with various shell thicknesses (5-80 nm) was reported by Kim *et al.*.[176] The gas sensor with a shell thickness of 30 nm demonstrated an enhanced gas response to the reducing gases, while, the pristine gas sensor revealed a better response to NO_2 gas. The degree of resistance modulation of the outer layer of Cu_2O which was directly exposed to air varied inversely with shell thickness. Therefore, a thicker shell was only partially modulated. In contrast, even though the very thin shells were completely experienced the resistance modulation, the fraction of the shell in comparison with total volume of C-S NWs was negligible and a low response was resulted. With considering the fraction of shell layers in the total volume of the n-p C-S NW (which was proportional to shell thickness), the response showed a bell-shaped curve with regard to shell thickness (Fig. 10), where a 30 nm thick shell showed the enhanced gas response. Also, for C-S NWs, the expansion of the outer Cu_2O layer was limited by the presence of the p-n interface, which acted as a blocking layer toward the expansion of the

outer layer of Cu_2O. Accordingly, less resistance modulation for NO_2 which is an oxidizing gas occurred, resulting in low response to it.

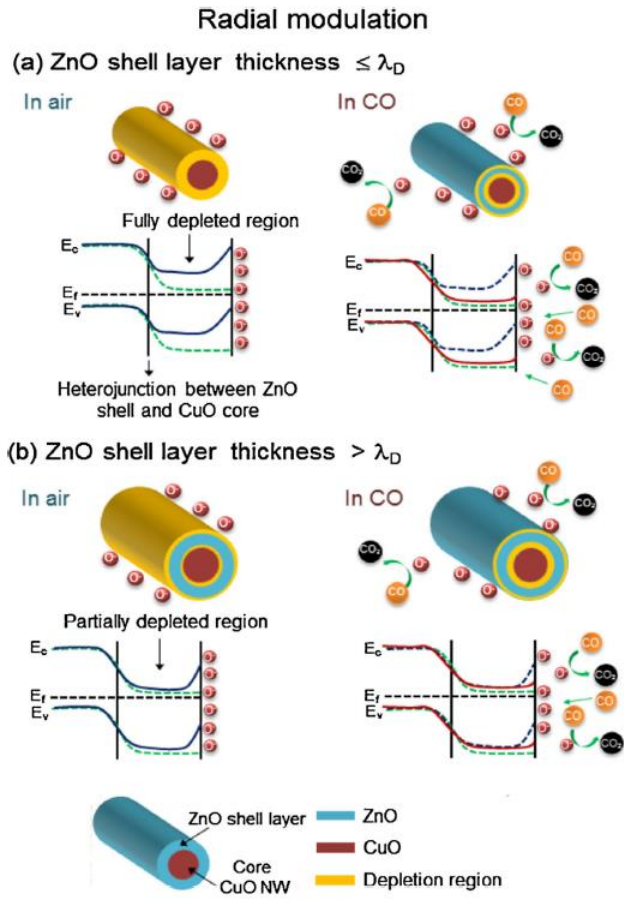

FIG. 9. The sensing mechanism of CuO-ZnO C-S NWs, (a) ZnO thickness smaller than Debye length (b) ZnO thickness thicker than Debye length.[175] Reproduced with permission Sensor. Actuat. B-Chem. **222,** 249-256 (2016). Copyright (2019) Elsevier.

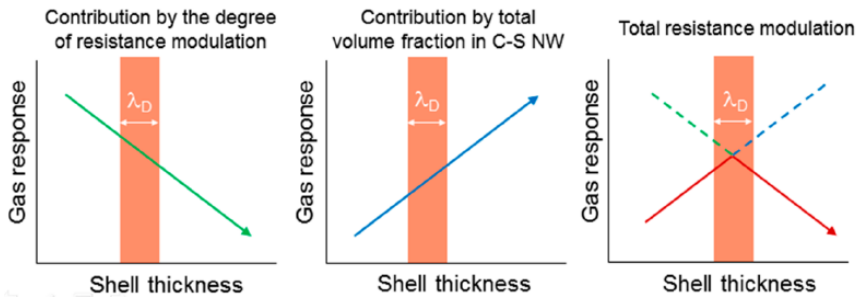

FIG. 10. The total resistance modulation of the C-S NWs in the presence of reducing gases.[176] " Reproduced with permission from ACS Appl. Mater. Interfaces **7**, 15351-15358 (2015). Copyright (2019) American Chemical Society.

In another study, the presence of an optimal shell thickness was also verified for SnO_2-ZnO C-S NWs (3.5-95 nm shell thickness), which was fabricated by VLS and ALD growth techniques.[177] The sensor with a shell thickness of 40 nm showed the highest response to the reducing gases. As presented in Fig. 11(a), the resistance due to the radial modulation of the electron-depleted shell was varied according to shell thickness. Also Fig. 11(b) displays the electric field smearing effect. For the shell layers thinner than λ_D, electron pathways were in both shell and core materials. This increases the resistance modulation in the C-S NWs. Even though a fully electron-depleted shell experienced a large resistance change, a noticeable portion of the electron pathways were through the inner core, resulting in a negligible resistance change for the C-S NW. Also, for thick shells, the resistance change in the C-S NWs upon exposure to reducing gases was determined only by the partial radial modulation of the electron-depleted shell and a low response was resulted. Fig. 11(c) shows how an optimal shell thickness can be resulted in the best sensing response.

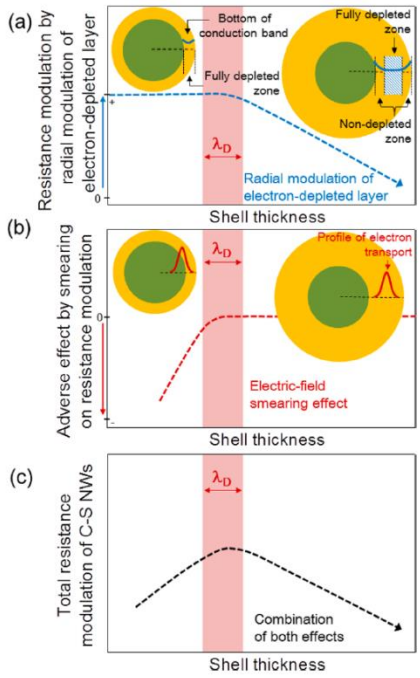

FIG. 11. (a) Resistance modulation by radial modulation of the electron-depleted shell (b) adverse effect by smearing on resistance modulation, and (c) total resistance modulation.[177]. Reproduced with permission from ACS Appl. Mater. Interfaces **6**, 8281-8287 (2014). Copyright (2019) American Chemical Society.

XII. Noble metal functionalized and heterojunction NW gas sensors

A very promising approach to enhance overall performance of gas sensors is functionalization or decoration with noble metals. In general, noble metals such as Pt,[178] Pd,[179] Au,[180] Rh[181] and Ag[182] enhance the adsorption of target gases and their subsequent interaction with the absorbed oxygen. Therefore, functionalized metal oxide NWs have attracted much attention.[183] Different methods, including gamma-ray irradiation,[184] UV-irradiation,[179] sputtering[185] and thermal evaporation,[186]can be used for introducing noble metals into oxide semiconductors.

When a noble metal is functionalized at the surface of metal oxides, due to the different work functions, charge transfers occur until the Fermi levels are equalized. Assuming that electrons migrate from metal oxides to the noble metals, which is a case often observed in noble metal oxide-functionalized gas sensors, electrons will accumulate in the noble metal and at the same time increases the width of electron depletion layer in the metal oxide. In fact, Schottky potential

barriers will be created in the interfaces between noble metal and metal oxide. Since noble metals have high number of mobile electrons, electrons can easily redistribute themselves to counteract any charge build-up near the heterojunction interface. The presence of negative charge on the surface of the noble metal can attract electronegative species such as oxygen gas.[187] In the presence of target gas, the height of Schottky potential barrier changes which leads to a resistance change of the gas sensor, contributing to the sensor signal.

Additionally, noble metal catalysts also have a chemical sensitization effect.[188] In chemical sensitization, noble metals with its catalytic activity cause an increase in the adsorption of gases onto the sensor surface (Fig. 12(a)). In fact, the gas molecules will first be adsorbed on the surface of noble metals and then will be split over on the surface of metal oxides. Spillover involves the transport of active species adsorbed a first surface onto another surface that is in intimate contact with the original adsorbing surface.[189] Oxygen or target gases can be adsorbed on the surface of noble metal and be dissociated into chemisorbed monatomic oxygen and final spilt over onto the surface of metal oxide. As an example, Pd can easily dissociate H_2 gas to atomic hydrogen. Then atomic hydrogen species can be adsorbed onto the surface of sensing material. Therefore, much more hydrogen atoms can be reacted with already adsorbed oxygen species, resulting in improved gas response, shorter response and recovery times as well as higher selectivity of the gas sensors.[190,191] However, too large particle size would reduce the surface-area of the gas sensor, and may significantly decreased the response of gas sensor.[192]Due to high catalytic activity of noble metals to a specific gas, many high selective NWs gas sensors with noble metal functionalization have been reported in the literature.[193,194]

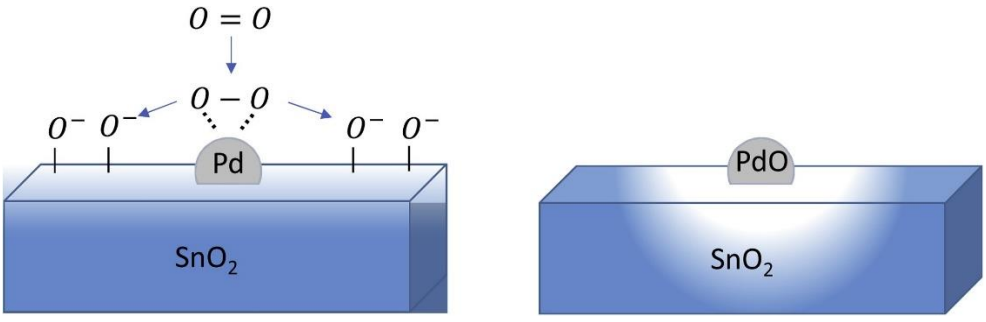

FIG. 12. (a) Chemical sensitization and (b) electronic sensitization effects of noble metals.[187] Reproduced with permission from Sensor. Actuat. B-Chem, **286**, 624-640 (2019). Copyright (2019) Elsevier.

In electronic sensitization, change of noble metal state in a metallic state to an oxidized state will cause significant change on the resistance of gas sensor (Fig. 12(b)). For example, Pd can be oxidized to PdO in oxidizing atmospheres, which causes a large modulation in resistance via electronic sensitization mechanisms.[187] Similarly, in air atmosphere generally some noble metals such as Ag and Pd become partially oxidized. When they are exposed to reducing gases, their electronic properties as well as work functions changes, which lead to a resistance modulation of gas sensor.[69] Also similar type of change has been reported in a hydrogen gas atmosphere where Pd has transformed to PdH_x, which is associated with a large resistance modulation.[157]

A disadvantage of noble metals is their high costs, which can significantly increase the sensor cost. In addition, noble metals can be poisoned in the presence of H_2S, SO_2, thiols and phosphorous.[195,196] Therefore, an alternative approach to increase the performance of NW gas sensor is realization of heterojunctions.

Heterojunction formation is a very popular method for fabrication of high performance gas sensors. In heterojunctions which can be n-n, n-p or p-p, since the Fermi level of a semiconducting material is different, the electrons at the higher energies will transfer to unoccupied lower-energy states until the Fermi energies be equalized. Accordingly, a net positive charge and a net negative charge in the materials in contact will be created. The flow of electrons will continue until the negative charge increase the energy of the electrons to prevent further flow of electrons.[187] A schematic representation of p-n and n-n junctions is shown in Fig. 13. Owing to the band bending, a potential energy barrier is established at this interface. Electrons must overcome this potential energy barrier in order to cross this interface.

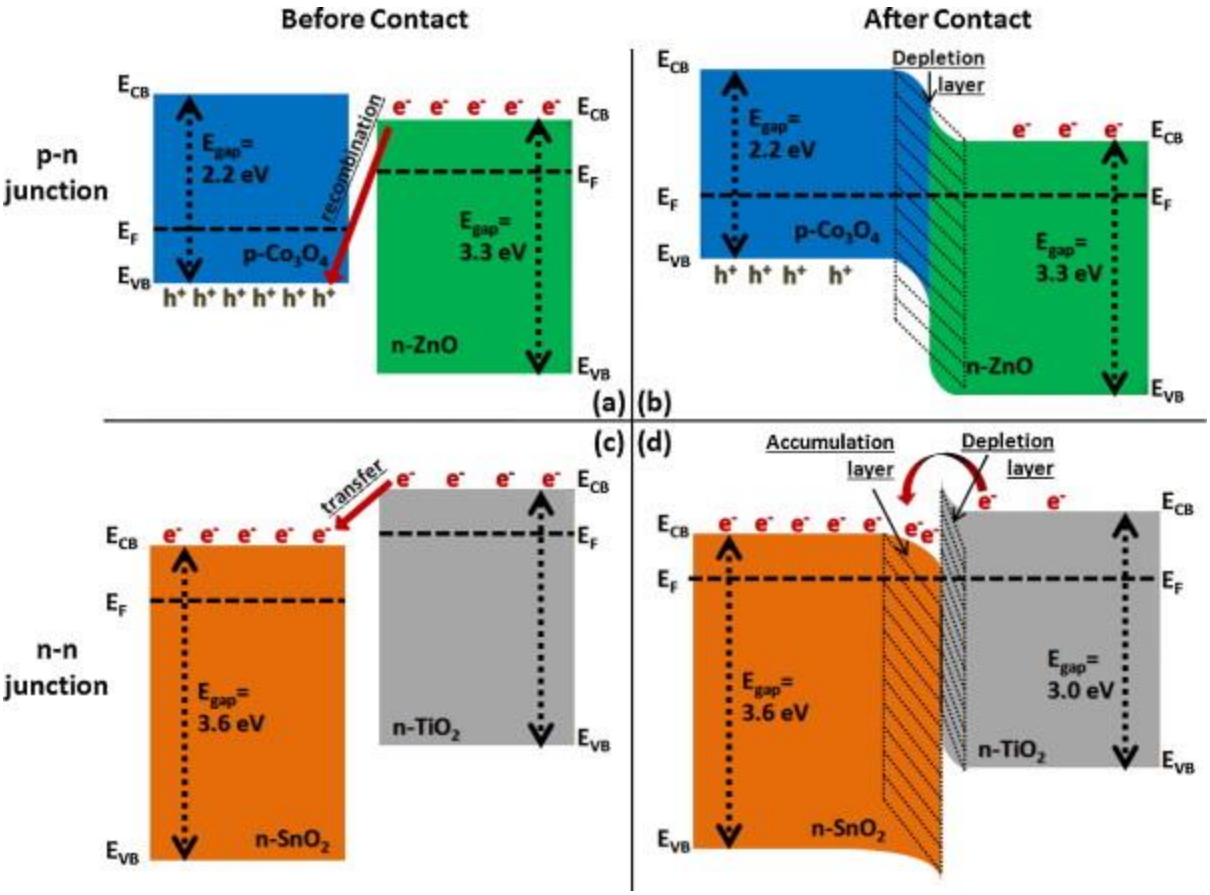

FIG. 13. (a) p-n junction before formation. (b) Depletion layer formed on both sides of p-n junction due to electron-hole recombination, (c) n-n junction before formation and (d) Depletion layer and accumulation layer.[197] Reproduced with permission from Sensor. Actuat. B-Chem. **204**, 250-272 (2014). Copyright (2019) Elsevier.

In heterojunction NWs, for example when an n-type NW sensor is in intimate contact with a p-type metal oxide, due to transfer of electrons from n-type NWs to p-type material, the diameter of the charge conduction channel inside of the n-type NWs decreases, and this leads to the increase of the air resistance. When the sensor is in an oxidizing gas atmosphere such as NO_2, a low response can be expected since there are no enough electrons in n-type NW to be withdrawn by NO_2 molecules. However, in the presence of a reducing gas, significant change in the diameter of charge conduction channel occurs, thus a high response is expected. This was confirmed by Na *et al.*,[198] in p-Cr_2O_3/ n- ZnO NWs gas sensor**.**

XIII. Low power consumption strategies: Light activation and self-heating operation

One of the major issues associated with the operating condition and stability of metal oxide NWs, is the relative high working temperature, which is required to enhance surface reactions to activate adsorbed oxygen and to enhance the reactivity with target gas. First Camagni *et al.*,[199] reported the UV enhanced sensing signal and then it was further confirmed that UV light could improve the sensing performances at room or low temperatures. Law *et al.*,[200] reported UV light illumination for enhanced gas response in NW gas sensors.

When metal oxide NW gas sensors are in dark environment at room temperature, only a few oxygen molecules can be adsorbed on the surface of gas sensor and are difficult to be desorbed. For the activation of the sensing layer, a minimum energy equal to the energy of the band-gap of the metal oxide is required. Illumination of sensor with a UV light with the photon energy equal or higher than the band gap of metal oxide NWs, can cause excitation of electrons from the valence to the conduction band. As a result, a large number of UV-induced electron-hole pairs will be generated in the NWs.

Also, it has been reported that using photons with excessive energies, above the threshold of the band gap, does not necessarily give better responses, since larger fraction of conduction electrons are lost with increasing energy as the result of inelastic scattering. Therefore, the maximum response can be corresponded to photons with energy close to the band gap of the metal oxide.[202] Since generally, wavelength of UV light is reported in the literature, the maximum wavelength of UV light which can be used for activation is as follows:

$$\lambda_{max} \leq hc/E_g \qquad (2)$$

where h is the Planck's constant (4.14×10^{-15} eV.s), c is the velocity of light (3.00×10^{8} m.s^{-1}) and E_g is the band gap.

UV illumination enhances the surface chemical activity through increasing the number of charge carriers in the conduction band, and accordingly it provides higher number of active sites on the surface. The target gas molecules then can be easily adsorbed and react with oxygen atoms on the surface of gas sensor. This leads to a significant change of the layer conductivity due to the

change in the number of electrons, and enables the gas concentration measurement by monitoring the conductance change over time.[201]

Two mechanisms are proposed for the direct desorption of adsorbates upon the exposure to UV radiation, direct excitation of a binding electron to the conduction band, or recombination with a photo-generated hole in the valence band. In other words, as the photons are irradiated to the surface, the photo-induced holes/electrons interact with the adsorbed oxygen causing to desorb oxygen ion species (photo-desorption) simultaneously along with the photo-induced electrons interaction with oxygen in the gas phase. This phenomenon continues to reach a new equilibrium state in which the rate of arrival of the holes and electrons to the surface becomes equal. Interaction and recombination of a hole with a binding electron of the layer could also break the bond and provide oxygen atom that is able to diffuse to the crystal surface, react with oxygen ions and form into O_2(g) and leave an oxygen vacancy behind.[201]

Consider the cross-section of a metal oxide NW such as ZnO, as schematically described in Fig. 14. Because of the built-in electric field in air, under UV illumination, some photo-generated holes on the surface react with adsorbed oxygen species and causing their desorption. At the same time, photo-induced oxygen species are created through the interaction between the oxygen molecules and the active photoelectrons. They are bound to the surface weakly as compared to chemisorbed oxygen species. In the target gas atmosphere, the change in resistance of ZnO sensor will increase under UV activation. Therefore, metal oxide NW gas sensor shows a high sensor a fast response-recovery time under UV light at lower sensing temperature.[202]

The pattern and intensity of the emitted UV light will seemingly affect the flow of the photons, which in turn influence the performance and sensing characteristics accordingly, due to the change in carriers' density incurred by photons interactions. Park *et al.*,[203] reported that the response of the ZnS-core/ZnO-shell NWs increased from 116 to 1180% with increasing UV light intensity from 0 to 1.2 mW/cm^2. It was found that the higher intensity of UV light may increase the number of electron-hole pairs, which significantly increase the charge carrier concentration, resulting in room-temperature operation and higher response of gas sensor. Another method of power consumption reduction is operation of gas sensor in the self-heating mode.

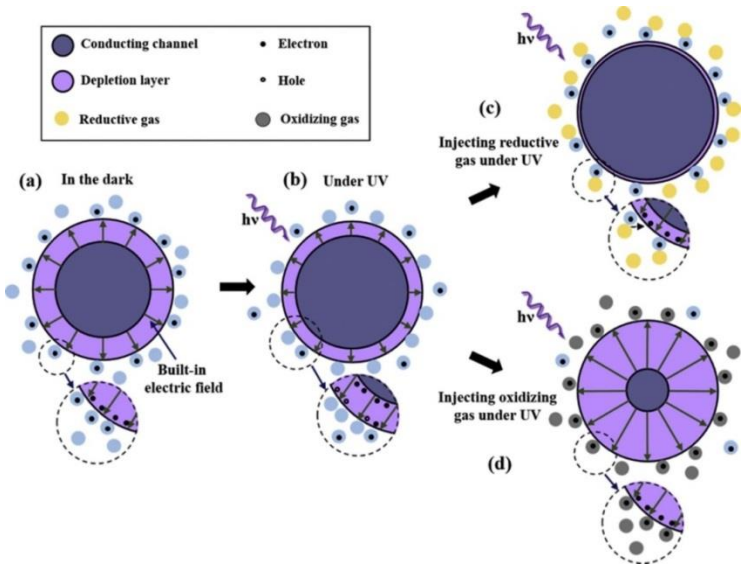

FIG. 14. Gas sensing mechanism of ZnO (a) in air, (b) in air under UV light, (c) in reducing gas under UV light and (d) in oxidizing gas under UV light.[202] Reproduced with permission from Sensor. Actuat. A-Phys. **267**, 242-261 (2017). Copyright (2019) Elsevier.

In some cases, for example in sensor arrays, UV illumination cannot result in a high response and they still need battery for their operation. Generally working temperature of gas sensors is high, which limit their usages in some places. However, when the number of sensors in a sensor array or a network is so high, replacing of individual batteries would represent a boring and difficult task. Furthermore, the battery materials have mostly potentially hazardous to health. Therefore, some novel approaches for decrease of power-consumption in gas sensors are needed.[204] Using Micromachining technology power consumption can be less than 30-50 mW, however, further reduction in power consumption is possible with self-heating strategy.[205]

Self-powered electronic devices were introduced by Xu *et al.* using ZnO NWs, in which a voltage of 1.26 V was produced by ZnO NWs, which was enough to recharge an AA battery.[206] Further studies showed that metal oxide NW gas sensors as well as metallic NWs[207,208] can work in self-heating mode with significant reduction of power consumed with a few tens of μW. Prades *et al.*[209] reported self-heated operation of SnO_2 NWs for NO_2 sensing with a power consumption of less than 20 μW which was remarkably lower than the 140 mW required for the external microheater. In self-heating operation, the small amount of power which used to probe the sensor resistance is sufficient to reach the optimum temperature of gas sensor (Fig. 15). First

time Salehi *et al.* applied an AC bias to self-heated SnO_2 gas sensor without external heating, demonstrated its successful operation for sensing application.[210] Self-heating gas sensors not only removes the external heaters, but also significantly reduces of the power consumption.[211] For self-heating gas sensors, it is generally accepted that the multiple NWs have a better performance than the single NW gas sensors. In fact, in the case of multiple NWs, since there are many NWs between the electrodes, the risk of sensor damaging due to failure of a NW decreases. Moreover, the conductivity range of multiple NW sensors permits application of much easier and cheaper electronic devices for operation of gas sensor. However, in a single NW gas sensor, the gas diffusion processes can be minimized, which can make the response and recovery times shorter.[212]

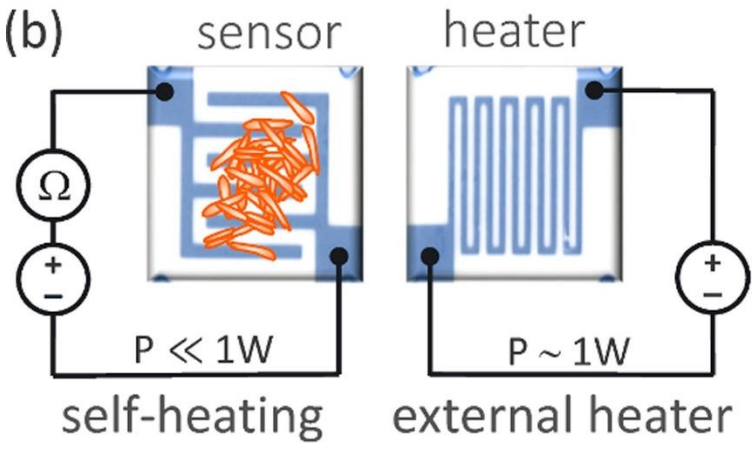

FIG. 15. Schematic representations gas sensors operating in self-heating and conventional mode[211]. Reproduced with permission from Sensor. Actuat. B-Chem. **256**, 797-811 (2018). Copyright (2019) Elsevier.

The main advantage of NWs for self-heating studies in comparison with thin film and thick film based gas sensors is their small thermal capacitance and significant reduction of thermal losses to the electrodes as well as the gas environment.[205] As a shortage of self-heating operation, it should be noted that during the Joule heating, sometimes the steady-state temperature is not homogeneous along the NW length, which prolongs the response time of self-heated gas sensors.[213] For self-heated gas sensors following points are important: (i) since the temperature rise is inversely proportional to the square radius of NWs, smaller diameter of NWs is better for

self-heating studies, (ii) thermal conductivity of NWs should be as high as possible and (iii) thermal loses with all elements in contact with the self-heated NWs should be decreased.[211]

Kim *et al.*[214] reported Pt-functionalized SnO_2-ZnO C-S NWs with a shell thickness of 10-85 nm in self-heating mode for gas sensing studies. Generally, for self-heating studies, the thermographs similar to Fig. 16 are reported to confirm the self-heating effect. The measured temperature increased with increasing shell thickness. There were three sources of Joule heating in the C-S NWs. First, because electrons passed though the ZnO grains, Joule heating occurred inside the ZnO grains (Fig. 17(a)). Second, the ZnO grain boundaries acted as another source of Joule heating (Fig. 17(b)). Third, since ZnO NWs were in intimate contact, the Joule heating occurred from the electrical currents through the ZnO-ZnO homojunctions (Fig. 17(c)). Increasing the shell thickness increased the diameter of the C-S NWs, and the probability of contact between NWs increased which led to a higher temperature. Accordingly, a higher C_7H_8 response in the sensor with an 85 nm-thick shell was resulted.

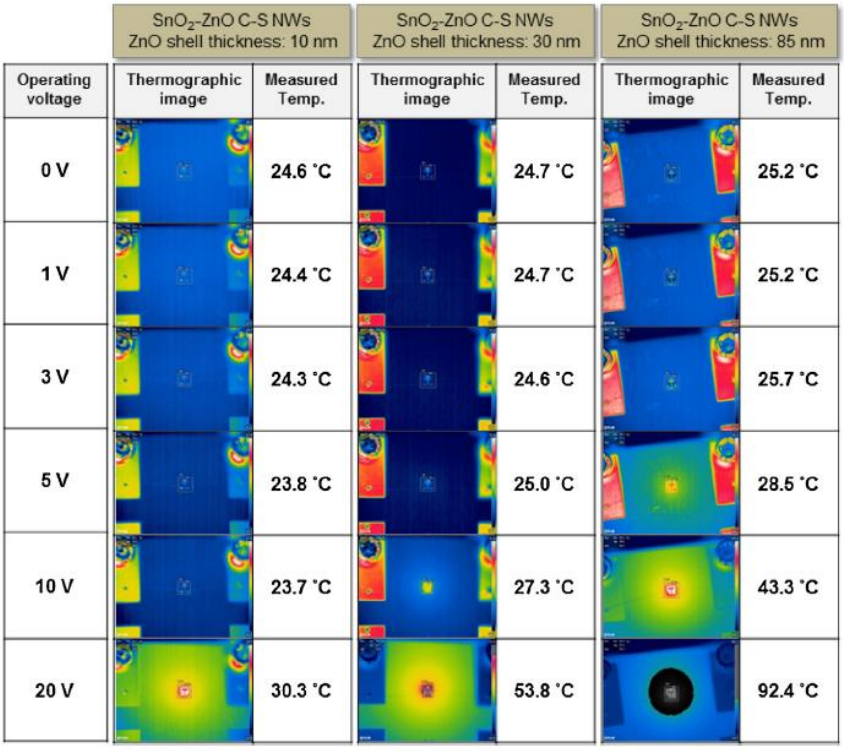

FIG. 16. Thermographs of Pt-functionalized SnO_2-ZnO C-S NW sensors at different shell thicknesses and applied voltages.[214] Reproduced with permission from Sensor. Actuat. B-Chem. **251**, 781-794 (2017). Copyright (2019) Elsevier.

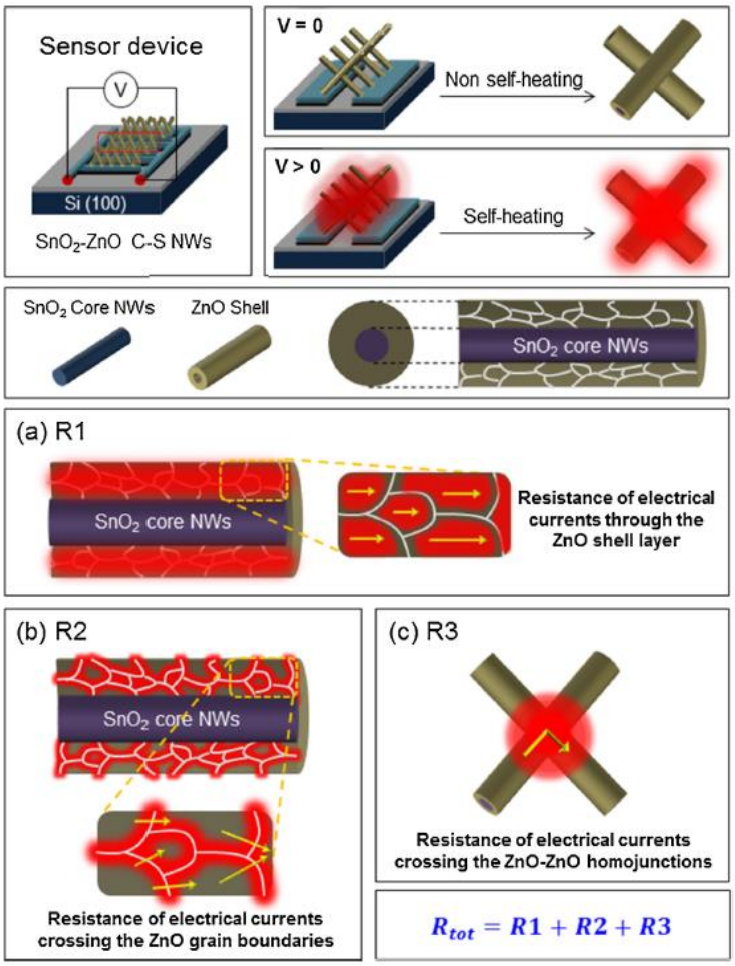

FIG. 17. Schematic of self-heated gas sensors and (a)-(c) sources of the generation of resistances in the C-S NWs.[214] Reproduced with permission from Sensor. Actuat. B-Chem. **251**, 781-794 (2017). Copyright (2019) Elsevier.

These results were also confirmed by another study. A novel self-heated CO gas sensor using Au-functionalized networked SnO_2-ZnO C-S NWs[215] was reported. The three sources of Joule heating in the SnO_2-ZnO C-S NWs were the resistance inside of ZnO grains, the resistance in grain boundaries and the resistances in the ZnO-ZnO homojunctions. It was found that by increasing the ZnO shell thickness, the response was increased. The power consumption at 3 and 20 V was 11.3 nW and 8.3 μW, respectively. Increasing the applied voltage enhanced the sensing response due to the self-heating effect within the sensor, and the sensors exhibited good performance without the need for an external heater. In a sensor with the optimal ZnO shell thickness of 80 nm, the responses for 50 ppm CO were 1.17 and 1.62 at 3 and 20 V, respectively.

The optimized ZnO shell, the catalytic effect of Au and the Joule effect contributed to the high response of gas sensor toward CO.[215]

Conclusions and outlook

Many toxic gases in our environment can be efficiently detected using metal oxide NW gas sensors. In this tutorial review paper, different aspects of metal oxide NW-based gas sensors were reviewed, from their synthesis methods to their sensing parameters and mechanisms. Single NW gas sensors can offer relatively high sensing performance and low LODs, due to their high surface area, excellent crystallinity and small diameter. However, their implantation in practical devices and the overall fabrication of gas sensors remains difficult. Because they present higher amounts of homo-and heterojunctions, multiple NWs and branched NWs offer higher sensing responses. In addition, they can be easily synthesized and implemented, for example by using VLS growth methods. Their surface functionalization with noble metals such as Pt, Pd, or Au can further increase the performance of these sensors in terms of sensitivity and selectivity. In heterojunction NWs, due to the presence of two materials with different work functions, the high modulation of the resistance at the interfaces can significantly increase the sensing response as well. In core/shell NWs, there is often an optimal shell thickness allowing for the highest gas sensing response. Using UV light, the gas sensors can work at a lower temperature, decreasing their power-consumption significantly. Another method for the reduction of power consumption is the use of self-heating strategy, in which NW gas sensors with extremely low powers can be realized. MOF nanomaterials can be used for the fabrication of highly selective gas sensors, as these porous structures act as selective membranes to certain gas molecules that can pass their small pores, resulting in higher selectivity. Based on this literature overview, it can be concluded that NWs have the potential to serve as the base of high performance, low-power consumption, and low cost gas sensors. In this regard, the optimization of amounts of noble metals, shell thickness, selection of appropriate MOF membrane, sensing temperature and sensing layer are important factors. It is expected that in near future, more sensitive, selective and stable gas sensors with fast response and short recovery times will be fabricated from metal oxide NWs.

References

[1]Y. Fu, Y. Nie, Y. Zhao, P. Wang, L. Xing, Y. Zhang and X. Xue, ACS Appl. Mater. Interfaces **7**, 10482-10490 (2015).

[2]S. J. Patil, A.V. Patil, C. G. Dighavkar, K. S. Thakare, R. Y. Borase, S. J. Nandre, N. G. Deshpande and R. R. Ahire, Front. Mater. Sci. **9**, 14-37 (2015).

[3]A. Baroutaji, T. Wilberforce, M. Ramadan and A. G. Olabi, Renew. Sust. Energ. Rev. **106**, 31-40 (2019).

[4]T. Hübert, L. Boon-Brett, G. Black, and U. Banach, Sensor. Actuat. B-Chem. **157**, 329-352 (2011).

[5]S. -C. Xu, Y. -M. Miao, C. Gao, R. -Y. Long, H. Chen, B. Zhao and S. -X. Wang, J. Clean. Prod. **208** 340-352 (2019).

[6]K. Wetchakun, T. Samerjai, N. Tamaekong, C. Liewhiran, C. Siriwong, V. Kruefu, A. Wisitsoraat, A. Tuantranont and S. Phanichphant, Sensor. Actuat. B-Chem. **160**, 580-591 (2011).

[7]A. Luengas, A. Barona, C. Hort, G. Gallastegui, V. Platel and A. Elias, Rev. Environ. Sci. Bio. **14** 499-522 (2015).

[8]M. Kuniavsky, Y. Bechor, M. Leitman and S. Efrati, Intens. Crit. Care Nur. **47**, 85-88 (2018).

[9]K. Thorsteinsson, R. N. Mortensen, C. Torp-Pedersen, B. Kjærgaard and J. J. Andreasen, PLoS ONE **14**, e0210767 (2019).

[10]S. M. Hosseininejad, H. Aminiahidashti, I. Goli Khatir, S. K. Ghasempouri, A. Jabbari and M. Khandashpour, J. Forensic Leg. Med. **53**, 87-96 (2018).

[11]S. Hammond and J. A. Phillips, Workplace Health Saf. **67**, 47-48 (2019).

[12]J. Garg, P. Krishnamoorthy, C. Palaniswamy, S. Khera, H. Ahmad, D. Jain, W. S. Aronow and W. H. Frishman, American J. Therap. **25**, 339-348 (2018).

[13]R. Kumar, O. Al-Dossary, G. Kumar and A. Umar, Nano-Micro Lett. **7**, 97-120 (2015).

[14]S. W. Lee, W. Lee, Y. Hong, G. Lee and D. S. Yoon, Sensor. Actuat. B-Chem. **255**, 1788-1804 (2018).

[15]T. -Y. Wong, J. Food Drug Anal. **25**, 235-244 (2017).

[16]S. K. Pandey, K. -H. Kim and K. -T. Tang, TRAC-Trend. Anal. Chem. **32**, 87-99 (2012).

[17]A. Mirzaei, S. S. Kim and H. W. Kim, J. Hazard. Mater. **357**, 314-331 (2018).

[18]M. Greabu, A. Totan, D. Miricescu, R. Radulescu, J. Virlan and B. Calenic, Antioxidants, **5**, 3 (2016).

[19]M. S. Kamal, S. A. Razzak and M. M. Hossain, Atmos. Environ. **140**, 117-134 (2016).

[20]A. Mirzaei, S. G. Leonardi and G. Neri, Ceram. Int. **42**, 15119-15141 (2016).

[21]H. Huang, Y. Xu, Q. Feng and D. Y. C. Leung, Catal. Sci. Technol. **5**, 2649-2669 (2015).

[22]A. Mirzaei, J. -H. Kim, H. W. Kim and S. S. Kim, J. Mater. Chem. C **6**, 4342-4370 (2018).

[23]F. Ren, L. Gao, Y. Yuan, Y. Zhang, A. Alqrni, O.M. Al-Dossary and J. Xu, Sensor. Actuat. B-Chem. **223**, 914-920 (2016).

[24]K. Kawamura, K. Kerman, M. Fujihara, N. Nagatani, T. Hashiba and E. Tamiya, Sensor. Actuat. B-Chem. **105**, 495-501 (2005).

[25]A. Majid and N. Kruspe, Curr. Biol. **28**, 409-413 (2018).

[26]C. Linster and O. Escanilla, Brain Res. **1709**, 33-38 (2019).

[27]N. Aguilar Martínez, G. Aguado Carrillo, P. E. Saucedo Alvarado, C. A. Mendoza García, A. L. Velasco Monroy and F. Velasco Campos, Rev. Med. Hosp. Gen. Méx. **81**, 268-275 (2018).

[28]X. Bao, E. Gjorgieva, L. K. Shanahan, J. D. Howard, T. Kahnt and J. A. Gottfried, Neuron **102**, 1066-1075 (2019).
[29]V. Grabe and S. Sachse, Biosystems, **164**, 94-101 (2018).
[30]J. P. McGann, Science **356**, eaam7263 (2017).
[31]Y. Bu, S. Er, J. W. H. Niemantsverdriet and H. O. A. Fredriksson J. catal. **357**, 176-187 (2018).
[32]A. -L. Moriaux, R. Vallon, B. Parvitte, V. Zeninari, G. Liger-Belair and C. Cilindre, Food Chem. **264**, 255-262 (2018).
[33]C. Becker, M. A. Jochmann and T. C. Schmidt, TRAC-Trend. Anal. Chem. **110**, 143-149 (2019).
[34]M. C. M. .M Souza, A. Grieco, N. C. Frateschi and Y. Fainman, Nat. Commun. **9**, 665 (2018).
[35]M. Meyyappan, Small 12, 21118-2129 (2016).
[36]I. Simon, N. Bârsan, M. Bauer and U. Weimar, Sensor. Actuat. B-Chem. **73**, 1-26 (2001).
[37]A. Hulanicki, S. Glab and F. Ingman, Pure Appl. Chem. **63**, 1247-1250 (1991).
[38]B. Liu, X. Chen, H. Cai, A. M. Mohammad, X. Tian, L. Tao, Y. Yang and T. Ren, J. Semicond. **37**, 021001 (2016).
[39]T. Liu, X. Zhang, L. Yuan and J. Yu, Solid State Ionics **283**, 91-102 (2015).
[40]C. Schwandt, R. V. Kumar and M. P. Hills, Sensor. Actuat. B-Chem. **265**, 27-34 (2018).
[41]Y. Wu, B. Yao, C. Yu and Y. Rao, Sensors **18**, 941 (2018).
[42]H. -E. Joe, H. Yun, S. -H. Jo, M. B. G. Jun and B. -K. Min, Int. J. Pr. Eng. Man-GT. **5**, 173-191 (2018).
[43]A. Mirzaei, J. -H. Kim, H. W. Kim and S. S. Kim, Appl. Sci. **9**, 1775 (2019).
[44]M. Chen, L. Zou, Z. Zhang, J. Shen, D. Li, Q. Zong, G. Gao, G. Wu, J. Shen and Z. Zhang, Carbon **130**, 281-287 (2018).
[45]T. Addabbo, A. Fort, M. Mugnaini, V. Vignoli, A. Baldi and M. Bruzzi, IEEE. T. Instrum. Meas. **67**, 722-730 (2018).
[46]A. S. Pranti, D. Loof, S. Kunz, M. Bäumer and W. Lang, Proceedings **2**, 927 (2018).
[47]A. Harley-Trochimczyk, T. Pham, J. Chang, E. Chen, M. A. Worsley, A. Zettl, W. Mickelson and R. Maboudian, Adv. Funct. Mater. **26**, 433-439 (2016).
[48]P. Tardy, J. -R. Coulon, C. Lucat and F. Menil, Sensor. Actuat. B-Chem. **98**, 63-68 (2004).
[49]C. Tsamis, A. G. Nassiopoulou and A. Tserepi, Sensor. Actuat. B-Chem. **95**, 78-82 (2003).
[50]X. Cao, Z. Zhang and X. Zhang, Sensor. Actuat. B-Chem. **99**, 30-35 (2004).
[51]A. Mirzaei and G. Neri, Sensor. Actuat. B-Chem. **237**, 749-775 (2016).
[52]Z. U. Abideen, J. -H. Kim, J. -H. Lee, J. -Y. Kim, A. Mirzaei, H. W. Kim and S. S. Kim, J. Korean Ceram. Soc. **54**, 366-379 (2017).
[53]K. C. Sekhar, S. S. C. Rao, Indian. J. Anaesth **58**, 350-352 (2014).
[54]C. Pollock, J. Avian Med. Surg. **30**, 386-391 (2016).
[55]W. H. Brattain and J. Bardeen, The Bell Sys. Tech. J. **32**, 1-41 (1953).
[56]G. Heiland, Z. Phys. **138**, 459-464 (1954).
[57]T. Seiyama, A. Kato, K. Fujiishi and M. Nagatani, Anal. Chem. **34**, 1502-1503 (1962).
[58]N. Taguchi, Japanese patent 23 (1962).
[59]K. Ihokura,J. Watson, *The Stannic Oxide Gas SensorPrinciples and Applications* (CRC press, Boca Raton, FL, 2017).
[60]C. Wang, L. Yin, L. Zhang, D. Xiang and R. Gao, Sensors **10**, 2088-2106 (2010).
[61]B. Zhang and P. -X. Gao, Front. Mater. **6**, 55 (2019).
[62]M. Drobek, J. -H. Kim, M. Bechelany, C. Vallicari, A. Julbe and S. S. Kim, ACS Appl. Mater. Interfaces **8**, 8323-8328 (2016)

[63]N. Barsan, D. Koziej and U. Weimar, Sensor. Actuat. B-Chem. **121**, 18-35 (2007).
[64]A. Šutka and K. A. Gross, Sensor. Actuat. B-Chem. **222**, 95-105 (2016).
[65]E. Joanni, R. Savu, P. R. Bueno, E. Longo and J. A. Varela, Appl. Phys. Lett. **92**, 132110 (2008).
[66]G. Korotcenkov, Mater. Sci. Eng. **139**, 1-23 (2007).
[67]H. -J. Kim and J. -H. Lee, Sensor. Actuat. B-Chem. **192**, 607-627 (2014).
[68]N. S. Ramgir, Y. Yang and M. Zacharias, Small **6**, 1705-1722 (2010).
[69]N. Yamazoe, G. Sakai and K. Shimanoe, Catal. Surv. Asia **7**, 63-75 (2003).
[70]M. Hübner, C. E. Simion, A. Tomescu-Stănoiu, S. Pokhrel, N. Bârsan and U. Weimar, Sensor. Actuat. B-Chem. **153**, 347-353 (2011).
[71]X. Gao and T. Zhang, Sensor. Actuat. B-Chem. **277**, 604-633 (2018).
[72]S. Park, G. -J. Sun, H. Kheel, W. I. Lee, S. Lee, S. -B. Choi and C. Lee, Sensor. Actuat. B-Chem. **227**, 591-599 (2016).
[73]G. Neri, Chemosensors **3**, 1-20 (2015).
[74]P. Mohankumar, J. Ajayan, R. Yasodharan, P. Devendran and R. Sambasivam, Measurement, **140**, 305-355 (2019).
[75]C. Di Natale, R. Paolesse, E. Martinelli and R. Capuano, Anal. Chim. Acta **824**, 1-17 (2014).
[76]M. Gardon and J. M. Guilemany, J. Mater. Sci. Mater. El. **24**, 1410-1421 (2013).
[77]A. Mashir and R. A. Dweik, Adv. Powder Technol. **20**, 420-425 (2009).
[78]G. Li, Z. Cheng, Q. Xiang, L. Yan, X. Wang and J. Xu, Sensor. Actuat. B-Chem. 283 590-601 (2019).
[79]N. Kazemi, B. Hashemi and A. Mirzaei, Process Appl. Ceram. **10**, 97-105 (2016).
[80]K. Arshak and I. Gaidan, Mater. Sci. Eng. **118**, 44-49 (2005).
[81]S. M. Kim, H. J. Kim, H. J. Jung, J. Y. Park, T. J. Seok, Y. H. Choa, T. J. Park and S. W. Lee, Adv. Funct. Mater. **29**, 1970039 (2019).
[82]A. Mirzaei, B. Hashemi and K. Janghorban, J. Mater. Sci. Mater. El. **27**, 3109-3144 (2016).
[83]J. -H. Lee, *Technological realization of semiconducting metal oxide–based gas sensors* (Elsevier, 167-216. 2019).
[84]M. Tiemann, Chem. Eur. J. **13**, 8376-8388 (2007).
[85]G. F. Fine, L. M. Cavanagh, A. Afonja and R. Binions, Sensors **10**, 5469-5502 (2010).
[86]A. Tsuruta, T. Itoh, M. Mikami, Y. Kinemuchi, I. Terasaki, N. Murayama and W. Shin, Materials **11**, 981 (2018).
[87]P. Rong, S. Ren and Q. Yu, Crit. Rev. Anal. Chem. **49**, 336-349 (2019).
[88]T. Wang, Y. Guo, P. Wan, H. Zhang, X. Chen and X. Sun, Small, **12**, 3748-3756 (2016).
[89]M. Alvarado, È. Navarrete, A. Romero, J. L. Ramírez and E. Llobet, Sensors **18**, 999 (2018).
[90]H. Ma, L. Yu, X. Yuan, Y. Li, C. Li, M. Yin and X. Fan, J. Alloy. Compd. **782**, 1121-1126 (2019).
[91]Y. Deng, *Semiconducting Metal Oxides for Gas Sensing* (Springer, 2019).
[92]A. K. Basu, P. S. Chauhan, M. Awasthi and S. Bhattacharya, Appl. Surf. Sci. **465**, 56-66 (2019).
[93]G. Korotcenkov and B. K. Cho, Sensor. Actuat. B-Chem. **244**, 182-210 (2017).
[94]G. Korotcenkov and B. K. Cho, Sensor. Actuat. B-Chem. **188**, 709-728 (2013).
[95]S. R. Morrison, Sensor. Actuat. **12**, 425-440 (1987).
[96]H. Tian, H. Fan, M. Li and L. Ma, ACS Sens. **1**, 243-250 (2016).
[97]B. Chen, S. Xiang and G. Qian, Acc. Chem. Res. **43**, 1115-1124 (2010).
[98]Y. Cui, B. Li, H. He, W. Zhou, B. Chen and G. Qian, Acc. Chem. Res. **49**, 483-493 (2016).

[99]T. Zhou, Y. Sang, X. Wang, C. Wu, D. Zeng and C. Xie, Sensor. Actuat. B-Chem. **258**, 1099-1106 (2018).
[100]M. Weber and M. Bechelany, Pure Appl. Chem. (Accepted).
[101]M. Weber, J. –H. Kim, J. –H. Lee, J. –Y. Kim, I. Iatsunskyi, E. Coy, M. Drogbek, A. Julbe, M. Bechelany, S and S. Kim, ACS. Appl. Mater. Interfaces **10**, 34765-34773 (2018)
[102]A. K. Srivastava, Sensor. Actuat. B-Chem. **96**, 24-37 (2003).
[103]X. Liu, S. Cheng, H. Liu, S. Hu, D. Zhang and H. Ning, Sensors **12**, 9635-9665 (2012).
[104]A. B. Gadkari, T. J. Shinde and P. N. Vasambekar, IEEE Sens. J. **11**, 849-861 (2011).
[105]N. Wu, B. Wang, C. han, Q. Tian, C. Wu, X. Zhang, L. Sun and Y. Wang, J. Mater. Chem. C **7**, 7299-7307 (2019).
[106]A. K. Nayak, R. Ghosh, S. Santra, P. K. Guha and D. Pradhan, Nanoscale, **7**, 12460-12473 (2015).
[107]J. Li, Y. Lu, Q. Ye, M. Cinke, J. Han and M. Meyyappan, Nano Lett. **3**, 929-933 (2003).
[108]M. Bonyani, J. K. Lee, G. -J. Sun, S. Lee, T. Ko and C. Lee, Thin Solid Films **636**, 257-266 (2017).
[109]D. R. Patil, L. A. Patil, P. P. Patil, Sensor. Actuat. B-Chem. **126**, 368-374 (2007).
[110]A. Mclaren, T. Valdes-Solis, G. Li and S. C. Tsang, J. Am. Chem. Soc. **131**, 12540-12541 (2009).
[111]Y. H. Navale, S. T. Navale, F. J. Stadler, N. S. Ramgir and V. B. Patil, Ceram. Int. 45 1513-1522 (2019).
[112]J. Lee, S. -H. Lee, S. -Y. Bak, Y. Kim, K. Woo, S. Lee, Y. Lim and M. Yi, Sensors **19**, 1903 (2019).
[113]N. V. Hoang, C. M. Hung, N. D. Hoa, N. V. Duy, I. Park and N. V. Hieu, Sensor. Actuat. B-Chem. **282**, 876-884 (2019).
[114]K. Wang, W. Wei, Z. Lou, H. Zhang and L. Wang, Appl. Sur. Sci. **479**, 209-215 (2019).
[115]X. Zhang, D. Song, Q. Liu, R. Chen, J. Hou, J. Liu, H. Zhang, J. Yu, P. Liu and J. Wang, J. Mater. Chem. C **7**, 7219-7229 (2019).
[116]I. Kortidis, H. C. Swart, S. S. Ray and D. E. Motaung, Sensor. Actuat. B-Chem. **285**, 92-107 (2019).
[117]F. Loghin, A. Abdellah, A. Falco, M. Becherer, P. Lugli and A. Rivadeneyra, Measurement **136**, 323-325 (2019).
[118]Y. Seekaew, A. Wisitsoraat, D. Phokharatkul and C. Wongchoosuk, Sensor. Actuat. B-Chem. **279**, 69-78 (2019)
[119]Y. Li, Z. Song, Y. Li, S. Chen, S. Li, Y. Li, H. Wang and Z. Wang, Sensor. Actuat. B-Chem. **282**, 259-267 (2019).
[120]F. Liu, X. Chen, X. Wang, Y. Han, X. Song, J. Tian, X. He and H. Cui, Sensor. Actuat. B-Chem. **291**, 155-163 (2019).
[121]H. Gao, Q. Yu, K. Chen, P. Sun, F. Liu, X. Yan, F. Liu and G. Lu, J. Colloid Interf. Sci. **535**, 458-468 (2019).
[122]H. Yang, X. Bai, P. Hao, J. Tian, Y. Bo, X. Wang and H. Liu, Sensor. Actuat. B-Chem. **280**, 34-40 (2019).
[123]F. Zhang, X. Dong, X. Cheng, Y. Xu, X. Zhang and L. Huo, ACS Appl. Mater. Interfaces **11**, 11755-11762 (2019).
[124]F. Qu, X. Zhou, B. Zhang, S. Zhang, C. Jiang, S. Ruan and M. Yang, J. Alloy. Compd. **782**, 672-678 (2019).

[125]J. Li, H. Liu, H. Fu, L. Xu, H. Jin, X. Zhang, L. Wang and K. Yu, J. Alloy. Compd. **788**, 248-256 (2019).
[126]Y. Li, X. Zhou, W. Luo, X. Cheng, Y. Zhu, A. M. El-Toni, A. Khan, Y. Deng and D. Zhao, Adv. Mater. Interfaces **6**, 1801269 (2019).
[127]V. K. Tomer, R. Malik, V. Chaudhary, A. Baruah and L. Kienle, *Noble Metal-Metal Oxide Hybrid Nanoparticles*, (Woodhead Publishing. 2019)
[128]Y. Liang, W. Liu, W. Hu, Q. Zhou, K. He, K. Xu, Y. Yang, T. Yu and C. Yuan, Mater. Res. Bull. **114**, 1-9 (2019).
[129]G. Ren, Z. Li, W. Yang, M. Faheem, J. Xing, X. Zou, Q. Pan, G. Zhu and Y. Du, Sensor. Actuat. B-Chem. **284**, 421-427 (2019).
[130]R. Yan, D. Gargas and P. Yang, Nat. Photonics **3**, 569 (2009).
[131]E. Comini and G. Sberveglieri, Mater. Today **13**, 36-44 (2010).
[132]Y. Yong, H. Cui, Q. Zhou, X. Su, Y. Kuang and X. Li, J. Phys. Chem. Solids. **127**, 68-75 (2019).
[133]X. Chen, C. K. Y. Wong, C. A. Yuan and G. Zhang, Sensor. Actuat. B-Chem. **177**, 178-195 (2013).
[134]Q. Wan, Q. H. Li, Y. J. Chen, T. H. Wang, X. L. He and J. P. Lin, Appl. Phys. Lett. **84**, 3654-3656 (2004).
[135]F. Patolsky and C. M. Lieber, Mater. Today **8**, 20-28 (2005).
[136]R. S. Wagner and W. C. Ellis, Appl. Phys. Lett. **4**, 89-90 (1964).
[137]D. -I. Suh, C. C. Byeon and C. -L. Lee, Appl. Surf. Sci. **257**, 1454-1456 (2010).
[138]S. V. Sivaram, H. Y. Hui, M. D. L. Mata, J. Arbiol and M. A. Filler, Nano Lett. **16**, 6717-6723 (2016).
[139]M. Ek and M. A. Filler, Accounts Chem. Res. **51**, 118-126 (2018).
[140]S. Kim, J. H. Bang, M. S. Choi, W. Oum, A. Mirzaei, N. Lee, H. -C. Kwon, D. Lee, H. Jeon, S. S. Kim and H. W. Kim, Met. Mater. Int. **25**, 805-813 (2019).
[141]Y. Wu and P. Yang, J. Am. Chem. Soc. **123**, 3165-3166 (2001).
[142]L. Yu, A. J. Riddle, S. Wang, A. Sundararajan, J. Thompson, Y. -J. Chang, M. E. Park, S. S. A. Seo and B. S. Guiton, Chem. Mater. **28**, 8924-8929 (2016).
[143]C. Cheng and H. J. Fan, Nano Today, **7**, 327-343 (2012).
[144]Q. Wan, J. Huang, Z. Xie, T. Wang, E. N. Dattoli and W. Lu, Appl. Phys. Lett. **92**, 102101 (2008).
[145]S. An, S. Park, H. Ko, C. Jin, W. I. Lee and C. Lee, Thin Solid Film **547**, 241-245 (2013).
[146]A. M. El-Toni, M. A. Habila, J. P. Labis, Z. A. ALOthman, M. Alhoshan, A. A. Elzatahry and F. Zhang, Nanoscale **8**, 2510-2531 (2016).
[147]P. Karnati, S. Akbar and P. A. Morris, Sensor. Actuat. B-Chem. **295**, 127-143 (2019).
[148]R. G. Chaudhuri and S. Paria, Chem. Rev. **112**, 2373-2433 (2011).
[149]D. Zappa, V. Galstyan, N. Kaur, H. M. M. M. Arachchige, O. Sisman and E. Comini, Anal. Chim. Acta **1039**, 1-23 (2018).
[150]J. Hämäläinen, M. Ritala and Markku Leskelä, Chem. Mater. **26**, 786-801 (2014).
[151] M. Weber, E. Coy, I. Iatsunskyi, L. Yate, P. Miele and M. Bechelany, Cryst. Eng. Comm. **19**, 6089-6094 (2017).
[152]M. Weber, I. Iatsunskyi, E. Coy, P.Miele, D.Cornu, M.Bechelany, Adv. Mater. Interfaces **5** (16), 1800056 (2018).
[153]M.J. Weber, M.A. Verheijen, A.A. Bol, W.M.M. Kessels Nanotechnology **26** (9), 094002, (2015)

[154]M. Leskelä and M. Ritala, Thin Solid Films **409**, 138-146 (2002).
[155]S. M. George, Chem. Rev. **110**, 111-131 (2010).
[156]C. Detavernier, J. Dendooven, S. P. Sree, K. F. Ludwig and J. A. Martens, Chem. Soc. Rev. **40**, 5242-5253, (2011).
[157]M. Weber, J. –Y. Kim, J. –H. Lee, J. –H. Kim, I. Iatsunskyi, E. Coy, P. Miele, M. Bechelany and S. S. Kim, J. Mater. Chem. A **7**, 8107-8116 (2019).
[158]M. Weber, I. Iatsunskyi, E. Coy, P. Miele, D. Cornu and M. Bechelany, Adv. Mater. Interfaces **5**, 180056 (2018).
[159]L. Liao, H. B. Lu, J. C. Li, C. Liu, D. J. Fu and Y. L. Liu, Appl. Phys. Lett. **91**, 173110 (2007).
[160]L. Liao, H. X. Mai, Q. Yuan, H. B. Lu, J. C. Li, C. Liu, C. H. Yan, Z. X. Shen and T. Yu, J. Phys. Chem. C **112**, 9061-9065 (2008).
[161]A. Kolmakov, D. O. Klenov, Y. Lilach, S. Stemmer and M. Moskovits, Nano Lett. **5**, 667-673 (2005).
[162]M. Tonezzer and N. V. Hieu, Sensor. Actuat. B-Chem. **163**, 146-152 (2012).
[163]Y. -J. Choi, I. -S. Hwang, J. -G. Park, K. J. Choi, J. -H. Park and J. -H. Lee, Nanotechnology **19**, 095508 (2008).
[164]O. Lupan, V. V. Ursaki, G. Chai, L. Chow, G. A. Emelchenko, I. M. Tiginyanu, A. N. Gruzintsev and A. N. Redkin, Sensor. Actuat. B-Chem. **144**, 56-66 (2010).
[165]M. Z. Asadzadeh, A. Köck, M. Popov, S. Steinhauer, J. Spitaler and L. Romaner, Sensor. Actuat. B-Chem. **295**, 22-29 (2019).
[166]D. Zhang, Z. Liu, C. Li, T. Tang, X. Liu, S. Han, B. Lei and C. Zhou, Nano Lett. **4**, 1919-1924 (2004).
[167]L. C. Tien, H. T. Wang, B. S. Kang, F. Ren, P. W. Sadik, D. P. Norton, S. J. Pearton and J. Lin, Electrochem. Solid-State Lett. **8**, G230-G232 (2005).
[168]J. H. Bang, M. S. Choi, A. Mirzaei, Y. J. Kwon, S. S. Kim, T. W. Kim and H. W. Kim, Sensor. Actuat. B-Chem. **274**, 356-369 (2018).
[169]S. S. Kim, H. G. Na, S. -W. Choi, D. S. Kwak and H. W. Kim, J. Phys. D Appl. Phys. **45**, 205301 (2012).
[170]H. W. Kim, H. G. Na, Y. J. Kwon, H. Y. Cho and C. Lee, Sensor. Actuat. B-Chem. **219**, 22-29 (2015).
[171]H. -S. Woo, C. -H. Kwak, J. -H. Chung and J. -H. Lee, ACS Appl. Mater. Interfaces **6**, 22553-22560 (2014).
[172]H. -S. Woo, C. -H. Kwak, J. -H. Chung and J. -H. Lee, Sensor. Actuat. B-Chem. **216**, 358-366 (2015).
[173]M. B. Gawande, A. Goswami, T. Asefa, H. Guo, A. V. Biradar, D. -L. Peng, R. Zboril and R. S. Varma, Chem. Soc. Rev. **44**, 7540-7590 (2015).
[174]P. K. Kalambate, Dhanjai, Z. Huang, Y. Li, Y. Shen, M. Xie, Y. Huang and A.K. Srivastava, Core@shell nanomaterials based sensing devices: A review, TRAC-Trend. Anal. Chem. **115**, 147-161 (2019).
[175]J. -H. Kim, A. Katoch and S. S. Kim, Sensor. Actuat. B-Chem. **222**, 249-256 (2016).
[176]J. -H. Kim, A. Katoch, S. -H. Kim and S. S. Kim, ACS Appl. Mater. Interfaces **7**, 15351-15358 (2015).
[177]S. -W. Choi, A. Katoch, G. -J. Sun, J. -H. Kim, S. -H. Kim and S. S. Kim, ACS Appl. Mater. Interfaces **6**, 8281-8287 (2014).

[178]M. S. Choi, A. Mirzaei, J. H. Bang, H. G. Na, C. Jin, S. S. Kim and H. W. Kim, J. Nanosci. Nanotechnol. **19**, 6647-6655 (2019).

[179]J. -H. Kim, A. Mirzaei, H. W. Kim and S. S. Kim Sensor. Actuat. B-Chem. **285**, 358-367 (2019).

[180]Z. U. Abideen, J. -H. Kim, A. Mirzaei, H. W. Kim and S. S. Kim, Sensor. Actuat. B-Chem. **255**, 1884-1896 (2018).

[181]R. Leghrib, T. Dufour, F. Demoisson, N. Claessens, F. Reniers and E. Llobet, Sensor. Actuat. B-Chem. **160**, 974-980 (2011).

[182]R. S. Ganesh, M. Navaneethan, V. L. Patil, S. Ponnusamy, C. Muthamizhchelvan, S. Kawasaki, P. S. Patil and Y. Hayakawa, Sensor. Actuat. B-Chem. **255**, 672-683 (2018).

[183]J. Huang and Q. Wan, Sensors **9**, 9903-9924 (2009).

[184]M. Tonezzer, J. -H. Kim, J. -H. Lee, S. Iannotta and S. S. Kim, Sensor. Actuat. B-Chem. **281**, 670-678 (2019).

[185]J. -H. Kim, Y. Zheng, A. Mirzaei and S. S.Kim, Korean J. Mater. Res. **26**, 741-750 (2016).

[186]M. G. Chung, D. -H. Kim, D. K. Seo, T. Kim, H. U. Im, H. M. Lee, J. -B. Yoo, S. -H. Hong, T. J. Kang and Y. H. Kim, Sensor. Actuat. B-Chem. **169**, 387-392 (2012).

[187]J. M. Walker, S. A. Akbar and P.A. Morris, Sensor. Actuat. B-Chem. **286**, 624-640 (2019).

[188]K. Suematsu, K. Watanabe, A. Tou, Y. Sun and K. Shimanoe, Anal. Chem. **90**, 1959-1966 (2018).

[189]W. C. Conner Jr and J. L. Falconer, Chem. Rev. **95**, 759-788 (1995).

[190]D. -T. Phan and G. -S. Chung, Sensor. Actuat. B-Chem. **204**, 437-444 (2014).

[191]Y. Luo, C. Zhang, B. Zheng, X. Geng and M. Debliquy, Int. J. Hydrogen Energ. **42**, 20386-20397 (2017).

[192]A. V. Singhal, H. Charaya and I. Lahiri, Crit. Rev. Solid State **42**, 499-526 (2017).

[193]H. -J. Cho, V. T. Chen, S. Qiao, W. -T. Koo, R. M. Penner and I. -D. Kim, ACS Sens. **3**, 2152-2158 (2018).

[194]K. Nguyen, C. M. Hung, T. M. Ngoc, D. T. T. Le, D.H. Nguyen, D. Nguyen Van and H. Nguyen Van, Sensor. Actuat. B-Chem. **253**, 156-163 (2017).

[195]A. Gremminger, P. Lott, M. Merts, M. Casapu, J. -D. Appl. Catal. B-Environ. **218**, 833-843 (2017).

[196]G. Korotcenkov, Sensor. Actuat. B-Chem. **107**, 209-232 (2005).

[197]D. R. Miller, S. A. Akbar and P. A. Morris, Sensor. Actuat. B-Chem. **204**, 250-272 (2014).

[198]C. W. Na, H. -S. Woo, I. -D. Kim and J. -H. Lee, Chem. Commun. **47**, 5148-5150 (2011).

[199]P. Camagni, G. Faglia, P. Galinetto, C. Perego, G. Samoggia and G. Sberveglieri, Sensor. Actuat. B-Chem. **31**, 99-103 (1996).

[200]M. Law, H. Kind, B. Messer, F. Kim and P. Yang, Angew. Chem. Int. Edit. **41**, 2405-2408 (2002).

[201]E. Espid and F. Taghipour, Crit. Rev. Solid State **42**, 416-432 (2017).

[202]L. Zhu and W. Zeng, Sensor. Actuat. A-Phys. **267**, 242-261 (2017).

[203]S. Park, S. Kim, H. Ko and C. Lee, J. Electroceram. **33**, 75-81 (2014).

[204]Z. L. Wang, Adv. Mater. 24, 280-285 (2012).

[205]G. Korotcenkov and B. K. Cho, Sensor. Actuat. B-Chem. **198**, 316-341 (2014).

[206]S. Xu, Y. Qin, C. Xu, Y. Wei, R. Yang and Z. L. Wang, Nat. Nanotechnol. **5**, 366 (2010).

[207]F. Yang, D. K. Taggart and R. M. Small **6**, 1422-1429 (2010).

[208]C. S. Prajapati, N. Bhat, Sensor. Actuat. B-Chem. **260**, 236-242 (2018).

[209]J. D. Prades, R. Jimenez-Diaz, F. Hernandez-Ramirez, S. Barth, A. Cirera, A. Romano-Rodriguez, S. Mathur and J. R. Morante, Appl. Phys. Lett. **93**, 123110 (2008).
[210]A. Salehi, Sensor. Actuat. B-Chem. **96**, 88-93 (2003).
[211]C. Fàbrega, O. Casals, F. Hernández-Ramírez and J. D. Prades, Sensor. Actuat. B-Chem. **256**, 797-811 (2018).
[212]E. Comini, Mater. Today **19**, 559-567 (2016).
[213]E. Strelcov, S. Dmitriev, B. Button, J. Cothren, V. Sysoev and A. Kolmakov, Nanotechnology **19**, 355502 (2008).
[214]J. -H. Kim, H. W. Kim and S. S. Kim, Sensor. Actuat. B-Chem. **251**, 781-794 (2017).
[215]J. -H. Kim, A. Mirzaei, H. W. Kim and S. S. Kim, Sensor. Actuat. B-Chem. **267**, 597-607 (2018).